Mather Caroline (Orcid ID: 0000-0003-0920-0642)

Geomorphic and hydrological controls on groundwater dolocrete formation in the semi-arid Hamersley Basin, northwest Australia

Caroline C. Mather[1*], David. J. Nash[2, 3], Grzegorz Skrzypek[1], Shawan Dogramaci[1, 4], Pauline F. Grierson[1]

[1]West Australian Biogeochemistry Centre and Ecosystems Research Group, School of Biological Sciences (M090), The University of Western Australia, 35 Stirling Highway, Crawley, WA 6009, Australia

[2]School of Environment and Technology, University of Brighton, Brighton, BN2 4GA, England

[3]School of Geography, Archaeology and Environmental Studies, University of the Witwatersrand, 1 Jan Smuts Avenue, Braamfontein 2000, Johannesburg, South Africa.

[4]Rio Tinto Iron Ore, 152-158 St. George's Terrace, Perth, WA 6000, Australia

*Corresponding author:

Caroline C. Mather, The University of Western Australia,

M090, 35 Stirling Highway, Crawley WA 6009, Australia

caroline.mather@research.uwa.edu.au

This article has been accepted for publication and undergone full peer review but has not been through the copyediting, typesetting, pagination and proofreading process which may lead to differences between this version and the Version of Record. Please cite this article as doi: 10.1002/esp.4704

Abstract

Groundwater dolocretes may exert an important geomorphic control on landscape evolution within sub-humid to arid regions. However, the geomorphic and hydrogeological settings of dolocrete remain poorly described. The hydrochemical conditions of dolomite precipitation in groundwater environments are also not well known. Classic models of dolocrete formation explain dolomite precipitation from highly evolved groundwaters at the terminus of major drainage but do not explain dolocrete distributed in regionally elevated landscapes, upgradient of major drainage. This study investigated the mineralogy, micromorphology and stable carbon and oxygen isotope compositions of three dolocrete profiles within a regionally elevated sub-basin of the Hamersley Ranges in the Pilbara region of northwest Australia. We sought to establish the environmental and hydrochemical conditions and present a model for dolocrete formation. We found that dolocrete formed within zones of emerging groundwater under saline-evaporitic conditions within internally draining sub-basins, most likely during the Late Miocene and Pliocene. Saline-evaporitic conditions were indicated by: i) the mineralogy, dominated by dolomite, palygorskite and smectite; ii) desiccation features and the presence of phreatic and vadose cements, indicative of a shallow fluctuating water table, and; iii) dolomite $\delta^{18}O$ values (median = -5.88‰). Dolomite precipitation was promoted by evaporation and CO_2 degassing from shallow Mg-rich groundwater. These factors appear to have been the major drivers of dolocrete development without a requirement for significant down-dip hydrochemical modification. Primary dolomite precipitation was possible due to the presence of microbial extracellular polymeric substances (EPS). EPS provided negatively charged nucleation sites, which bound Mg^{2+}, overcoming kinetic effects. High microbial activity within groundwater systems suggest these processes may be

important for dolocrete formation worldwide and that groundwater dolocretes may be more pervasive in landscapes than currently recognised.

Keywords: dolomite, stable isotopes, chemical sediments, microbial EPS, landform evolution

Introduction

Sediments and regolith indurated by eodiagenetic cements, such as silcrete, calcrete and ferricrete, are strongly resistant to erosion and form a major geomorphic control on landform evolution in the tropics and subtropics (Thomas, 1994; Pain and Ollier, 1995). Such sediments can form as hardpans within soils as a consequence of pedogenic processes, or develop as several to tens of metres thick profiles associated with precipitation from groundwater within drainage and palaeodrainage systems (i.e. groundwater duricrusts). Groundwater associated duricrusts can be volumetrically vast and extend for tens of kilometres along drainage channels. Of particular prevalence are calcretes and dolocretes, which are common in many sub-humid to arid landscapes (Goudie, 1972; Carlisle, 1983; Wright and Tucker, 1991). The accumulation and preservation of carbonate minerals within calcretes and dolocretes reflects a range of near surface physiochemical processes. Carbonate duricrusts may also form an archive of palaeoenvironmental information, as the stable isotope signatures of carbonate minerals reflect environmental conditions at the time of their initial deposition and during subsequent diagenesis (cf. Wright, 2007).

Calcretes are widely distributed within drainage and palaeodrainage systems, as calcite saturation is readily reached within relatively dilute groundwaters (Hutton and Dixon, 1981; Arakel and McConchie, 1982; Humphreys, 2001). In contrast, dolocretes

are less frequently reported; documented examples almost exclusively occur down-gradient of calcretes at the terminus of drainage systems proximal to saline or playa lakes (Mann and Deutscher, 1978; Arakel and McConchie, 1982; Armenteros et al., 1995). Dolomite precipitation is inhibited at surface temperatures and pressures and may not even occur when supersaturated in solution (Morrow, 1982; Land, 1998). The dominant factor inhibiting dolomite precipitation is the high enthalpy of the Mg^{2+} double hydration shell (Lippman, 1973; Morrow, 1982). In addition, low CO^{3-} activity relative to HCO^{3-} typical in most natural waters may be limiting to crystal growth. As such, conditions that favour dolomite precipitation are primarily (i) a high ratio of Mg to Ca in solution and (ii) high CO_3^{2-} activity (Lippman, 1973; Morrow, 1982).

Dolomite may form by replacement of a carbonate precursor (dolomitization) or by primary precipitation (direct nucleation). Primary dolomite has been recognised in various settings, including lacustrine (e.g. Petersen et al., 1963; Von der Borch, 1976; Garcia del Cura et al., 2001), saline evaporitic (e.g. hypersaline lagoons/playas and sabkhas; Curtis et al., 1963; Vasconcelos and McKenzie, 1997; Bontognali et al., 2010) and phreatic environments (Khalaf, 1990; Spötl and Wright, 1992; Alonso-Zarza et al., 2016). Models of dolocrete formation demonstrate the importance of hydrochemical modification along the flow path, primarily from evaporative concentration and the precipitation of calcite upgradient, increasing salinity of groundwater and the Mg/Ca ratio (Eugster, 1980). Outgassing of CO_2 at groundwater discharge zones, as well as mixing of fresh and saline groundwaters around saline lakes (El-Sayed et al., 1991; Colson and Cojan, 1996; Khalaf et al., 2017), may result in increased alkalinity and therefore CO_3^{2-} activity relative to HCO_3^-, promoting dolomite precipitation (Eugster, 1980; Morrow, 1982). However, the mechanisms of dolomite precipitation remain poorly understood and recent research has indicated

that microbial activity may be an important control on primary dolomite formation (Petrash et al., 2017).

Groundwater ecosystems constitute the largest global depository for terrestrial microbial biomass (Griebler and Lueders, 2009); as such, dolocretes forming in the phreatic zone may provide new information on the processes controlling dolomite precipitation within surficial terrestrial environments. Microbial activity, including sulphate-reducing bacteria, may act as catalysts for dolomite precipitation (Vasconcelos et al., 1995; Van Lith et al., 2002; Wacey et al., 2007; Bontognali et al., 2012). Organic matter containing a high density of carboxyl-groups may also increase rates of dolomite precipitation (Zhang et al., 2012; Roberts et al., 2013). In particular, extracellular polymeric substances (EPS) excreted by microbes have been increasingly linked to dolomite formation in terrestrial settings (Bontognali et al., 2010; Bontognali et al., 2014a; Zhang et al., 2015). EPS provides negatively charged nucleation sites, which dewater and bind Mg^{2+}, overcoming the high hydration energy of Mg^{2+} (Roberts et al., 2013; Zhang et al., 2015). Consequently, it might be expected that microbes and or EPS are also key drivers of dolocrete development.

The specific conditions in which dolomite in groundwater environments may precipitate and the extent of groundwater dolocretes across a range of landscape settings are not well known. The majority of detailed studies of terrestrial dolomite formation have focussed on lacustrine environments, often within saline coastal lake systems or playas (Last, 1990). However, there has been less attention given to groundwater-formed duricrusts and consequently the geomorphic and hydrogeological settings of groundwater dolocrete remain poorly described. Further, where studies of groundwater dolocretes have been undertaken, they are mostly based on extensive duricrusts within large, low elevation palaeodrainage features (e.g. Mann and Horwitz,

1979; Khalaf, 1990; Spötl and Wright, 1992; Armenteros et al., 1995). Under the right conditions, it should be possible for extensive dolocrete deposits to develop in smaller sub-basins in regional upland settings; such duricrusts may exert an important local geomorphic control on the landscape and influence both surface and sub-surface processes.

In this study, we provide the first detailed investigation of groundwater dolocrete within a regionally elevated (upland) sub-basin of the geological province known as the Hamersley Basin, in the semi-arid Pilbara region of northwest Australia. Our approach included a systematic mineralogical and micromorphological characterisation of the dolocrete as well as stable carbon and oxygen isotope analyses of groundwater dolocrete profiles. Our objectives were to: 1) define the geomorphic setting of the upland dolocrete; 2) establish the environmental and hydrochemical conditions resulting in dolomite formation; and 3) develop a model of dolocrete formation within a smaller sub-basin setting. The Hamersley Basin is an ideal location for this study for several reasons. Thick groundwater calcretes and dolocretes occur at a range of elevations across the landscape; these include the upper reaches of drainage systems in areas of emerging groundwater, as well as in the lowland terminal Fortescue Marsh (Barnett, 1980; Barnett and Commander, 1985; Mather et al., 2018). Mineralogical data also indicates that dolomite is the predominant carbonate mineral in most locations. This basin-wide distribution of dolocretes suggests that regional climatic, hydrologic and hydrochemical conditions promoted dolomite precipitation.

Geological and geomorphological context

The Hamersley Basin

The ~100,000 km^2 Hamersley Basin (Figure 1) is occupied by the Archaean to Proterozoic Mount Bruce Supergroup, which unconformably overlies the Archaean granite-greenstone basement rocks of the Pilbara Craton (Trendall, 1968). The site for this study is situated on the Hamersley Group (ca 2.63-2.45 Ga), a ~2.5 km thick sequence of banded iron formations interstratified with dolomite, shale, argillite and various igneous rocks (Trendall and Blockey, 1970), part of the Mount Bruce Supergroup (Trendall et al., 2004). The modern landscape developed within the Precambrian Hamersley Basin is strongly influenced by the structure and differential susceptibility to weathering of its geology. Topographic highs are primarily composed of resistant banded iron formation, whereas valleys are underlain by more easily eroded dolomite and shale units, largely of the Wittenoom Formation (Twidale et al., 1985). Where the Precambrian basement rocks are relatively undeformed and bedding is sub-horizontal, the landscape comprises flat topped hills and plateaus incised by deep dendritic valleys (Killick et al., 2008). Increasing deformation in the southern part of the basin has resulted in the ridge and valley topography of the Hamersley Ranges, due to tight, overturned E-W trending folds (Killick et al., 2008; Kneeshaw and Morris, 2014).

Dissection of the landscape during the Late Cretaceous and early Paleogene resulted in the incision of the major drainage features (Bowler, 1976; Twidale et al., 1985; Alley et al., 1999), interpreted to have been mature river systems extending over much of the basin (>100 km long), including the Fortescue River (Morris, 1993). Landscape evolution is characterised by periods of intense weathering followed by stripping (Kneeshaw and Morris, 2014). A prevailing warm and humid climate during much of the Paleogene promoted strong physical and chemical weathering such that deep regolith profiles developed (Twidale et al., 1985; Killick et al., 2008). A phase of

stripping and sediment aggradation within deeply incised valleys and drainage channels commenced in the Eocene (Macphail and Stone, 2004; Morris and Ramanaidou, 2007); few vestiges of the earlier landscape remain. Another deep weathering phase occurred during the early- to mid-Miocene, forming deep regolith cover across the landscape (Kneeshaw and Morris, 2014). Sinuous drainage channels often >100 m deep were incised and subsequently filled with iron-rich sediments and clays (Morris and Ramanaidou, 2007). Remobilisation and precipitation of iron within ferruginous channel sediments resulted in the formation of channel iron deposits under warm and increasingly dry conditions during the Miocene (MacPhail and Stone, 2004; Morris and Ramanaidou, 2007; Heim et al., 2006; Schmidt and Williams, 2017).

Calcrete and dolocrete duricrusts developed within channel and valley sediments following a shift to aridity and slightly cooler conditions in the Late Miocene (Barnett and Commander, 1985; Humphreys, 2001; Kneeshaw and Morris, 2014). Calcrete has been reported overlying channel iron deposits, particularly within upstream constrictions in strike valleys and within the Oakover Formation in the NE Pilbara (Morris and Ramanaidou, 2007; Kneeshaw and Morris, 2014), although mineralogical data suggest that many of the reported “calcretes” are dolomitic (Barnett, 1980; Barnett and Commander, 1985; Hewson et al., 2006; Haest et al., 2012). Dolocrete also occurs throughout the Fortescue Valley palaeodrainage, within the Millstream Formation of the Western Fortescue Valley (Barnett and Commander, 1985) and within the Fortescue Marsh to the east (Mather et al., 2018). Kneeshaw and Morris (2014) assigned the “calcrete” as the boundary between mid- to late-Miocene detrital deposition (CzD2), including channel iron deposits, and Pliocene to Quaternary detrital deposition (CzD3), constraining the major calcrete and dolocrete development to the late Miocene-Pliocene. A second phase of dolocretization during the Pleistocene was

also identified within the Fortescue Valley sediments (Barnett, 1980; Mather et al., 2018) but has not been reported in other locations and is not considered to be as widespread or voluminous as the Miocene-Pliocene calcretes and dolocretes.

Erosion of the landscape ongoing since the Pliocene (Kneeshaw and Morris, 2014) has dissected alluvial sediments and resulted in relief inversion, where indurated deposits (e.g. channel iron deposits, silcrete and calcrete) formed in valleys or channels may remain in the landscape as positive relief (Twidale, 1985). Dolocrete/calcrete outcrops are observed in areas of groundwater emergence along structural boundaries, and large outcrops tens of km^2 are notable in the upper reaches of creek systems (e.g. Weeli Wolli, Coondiner and Marillana Creeks; Figure 1). Outcrops are also observed along valley flanks or as eroding mounds, extruding above the valley floor (Figure 2). The modern landscape comprises the vestiges of earlier stripped landscapes, large areas of exposed bedrock, and complex palaeodrainage patterns and relief inversion, with valleys containing Eocene to Holocene alluvium, colluvium and chemical sediments.

Site geomorphology and dolocrete distribution

The study area is located in the upper reaches of the ephemeral Coondiner Creek system within a sub-basin of the Hamersley Ranges (Figure 1); hereafter referred to as the Coondiner sub-basin. The landscape is characterised by strongly developed ridge and valley topography; elevation varies from ~600 m above sea level (asl) in the valleys up to ~700-850 m along ridges, with the highest peak of 1250 m at Mount Meharry (Figure 1). Major drainage is primarily aligned with NE trending faults. Creeks exit into large alluvial fan systems at the base of the ranges (~500 m asl), which in turn

feed into the Fortescue Marsh, the terminal basin of the Upper Fortescue River Catchment (Figure 1; Rouillard et al., 2015).

Groundwater within the Coondiner sub-basin is primarily hosted in the dolomitic Wittenoom Formation, which comprises an extensive regional fractured aquifer system of ~300 to 600 m thick, characterised by Mg, Ca and HCO_3 rich groundwater (Dogramaci et al., 2012). Within the study area, groundwater flows generally eastward along strike valleys, shallowing as the aquifer is pinched out along the main NE fault boundary and creek channel by juxtaposition with relatively impermeable units. Locally, the Wittenoom Formation aquifer is connected to overlying surficial unconfined alluvial aquifers of Cenozoic sediments and within locally permeable mineralised banded iron formation. Emerging groundwater flows into the shallow alluvium overlying and east of the fault and north-eastward within alluvium connecting with Coondiner Creek. Outflow occurs at Eagle Rock Falls (Figure 3C) where alluvium thins out to expose volcanic rocks. Modern groundwater levels range from ~45 m depth below ridges, to ~25 m within valley sediments, and shallows to ~12 m in alluvium within the Coondiner Creek drainage.

Approximately ~12 km^2 of dolocrete is exposed at the surface within the Coondiner sub-basin where an upper NE trending creek channel turns sharply eastward along a lithological boundary, before merging with smaller tributaries and forming the main north-easterly Coondiner Creek channel (Figure 3B). The dolocrete outcrop is relatively flat (~650-660 m a.s.l) and is incised by small drainage lines connecting to Coondiner Creek (Figure 3A and C). Bedrock lithology varies within this area due to tight folding, and includes dolerite of the Weeli Wolli Formation, banded iron formation, shale of the Brockman Iron Formation, and shale, chert and dolomite of the Wittenoom Formation (Trendall and Blockey, 1970). The lateral sub-surface extent of dolocrete is

not fully known; available drill core data suggests the main body of dolocrete may extend several kilometres west and southwest of the outcrop. However, within the main strike valleys, the distribution of dolocrete is heterogeneous and patchy. Dolocrete of up to 30 m thick has been identified in a number of locations within the strike valleys, buried by ~20-50 m of transported sediments. These sediments are often dominated by clay or detrital host materials (CzD2) and are not fully dolocretised. The dolocrete in the strike valley is sometimes directly upon dolomite bedrock, whereas in other locations it is underlain by alluvium.

Sampling and analytical methods

Extensive mining activity in the Hamersley Basin has made it possible to improve knowledge of the surface and sub-surface geology, including duricrusts, a feat rarely possible in remote inland continental settings in Australia. The study utilises three diamond drill cores (cores 010, 009 and 015) extracted within 1 km of each other on the south-eastern corner of the Coondiner Creek dolocrete outcrop (see Figure 3C for locations). Each core penetrated the complete profile of the in-situ sub-surface dolocrete. This study thus contrasts with many analyses of duricrusts that have focused on outcropping occurrences (Nash and McLaren, 2003; Khalaf et al., 2017). Exposure of dolocrete to the vadose zone, or more significantly sub-aerial conditions, will commonly result in chemical, mineralogical and or textural changes (e.g. dedolomitization, dissolution-precipitation processes, pedogenic carbonate formation, and bioturbation), such that analysis of outcropping occurrences may not accurately reflect the environmental conditions of dolomite formation (Khalaf and Abdal, 1993; Arenas et al., 1999; Alonso-Zarza, 2003).

Petrographic analysis was completed on 60 polished thin sections using a compound binocular microscope and transmitted light microscope. Scanning electron microscopy (SEM) observations and semi-quantitative elemental analysis were performed on the thin sections and 15 fresh dolocrete samples using a Verios XHR fitted with an Oxford instruments SDD-X-Max energy dispersive X-Ray (EDX) spectrometer.

A total of 60 core sections were sampled for mineral analysis using x-ray diffraction (XRD). A further 9 carbonate sub-samples were analysed by XRD to confirm carbonate mineralogy for isotope analysis (see below). For quantitative XRD analysis, approximately 1.5g of each oven dried sample (105°C) was ground for 10 minutes in a McCrone micronizing mill under ethanol. The resulting slurries were oven dried at 60°C then thoroughly mixed with an agate mortar and pestle before being lightly back pressed into stainless steel sample holders for analysis. XRD patterns were recorded with a PANalytical X'Pert Pro Multi-purpose Diffractometer using Fe filtered Co Ka radiation, variable divergence slit, 1° anti-scatter slit and fast X'Celerator Si strip detector. The diffraction patterns were recorded in steps of 0.017° 2 theta with a 0.5 second counting time per step. Quantitative analysis was performed on the XRD data from all bulk samples using the commercial package SIROQUANT from Sietronics Pty Ltd. The results are normalised to 100%, and hence do not include estimates of unidentified or amorphous materials. The molar proportion of $CaCO_3$ in dolomite and Mg substitution in calcite was calculated from *a* and *c* unit cell data determined by Rietveld analysis (Bischoff et al., 1983; Reeder and Sheppard, 1984).

Forty-eight bulk dolocrete samples and 103 sub-samples were analysed for $\delta^{13}C$ and $\delta^{18}O$ values of carbonate. The sub-samples targeted more pure materials containing carbonate, primarily different matrix and cements with various colour or textural properties (e.g. cemented vs. powdery). Samples were analysed using a GasBench II

coupled with a Delta XL Mass Spectrometer (Thermo-Fisher Scientific). Samples of carbonate powder were reacted with 0.05 mL of 100% orthophosphoric acid at 50°C in helium atmosphere (Paul and Skrzypek, 2007). To obtain calcite and dolomite stable isotope compositions, each sample was analysed twice using different reaction times: 24 h for total carbonates (calcite and dolomite) and 15 minutes for calcite only. The $\delta^{13}C$ and $\delta^{18}O$ values of carbonate samples were normalised to VPBD scale using international reference materials (LSVEC = -46.6‰ and NBS 18 = -5.01‰; NBS 19 = 1.95‰ for $\delta^{13}C$ and NBS 18 = -23.01 ‰ and NBS 19 = -2.2 ‰ for $\delta^{18}O$), following a three and two point normalisation, and reported in per mil (Brand et al., 2014; Skrzypek, 2013). The combined uncertainty of stable isotope analyses is <0.10‰ for $\delta^{13}C$ and <0.15‰ for $\delta^{18}O$ (1 standard deviation). The dolomite stable isotope composition of mixed carbonate samples was calculated using a stable isotope mass balance model and the difference between the $\delta^{13}C$ and $\delta^{18}O$ values of total carbonates and calcite. The relative proportions of calcite and dolomite in samples were calculated based on sample weights and amount of produced CO_2 recorded as the area of all peaks for molecular masses *m/z*44-45-46. These values were in agreement with the proportion of dolomite determined by XRF and XRD. The $\delta^{18}O$ values were measured versus calcite standards and were recalculated for dolomite samples using acid digestion isotope fractionation factors (Das Sharma et al., 2002).

Results

Profile characteristics and host sediments

The dolocrete profiles ranged from ~11 m thick (core 010, overlying banded iron formation of the Brockman Iron Formation) to ~22 m thick (core 015, overlying McRae Shale) (Figure 4). Host sediments include ~8-14 m of alluvial and lacustrine sediments and underlying regolith and saprock (Figure 4). The detrital host sediments are

consistent with the clay-dominated CzD2 sediments described by Morris and Ramanaidou (2007) and Kneeshaw and Morris (2014), and are composed of clay to silt alluvium, containing varying proportions of clay aggregates, silcrete fragments and Fe-oxide cemented pisoliths and gravels.

The detrital host sediments within core 010 consist of ~8 m of alluvial to lacustrine clay underlain by ~3 m of conglomerate. The alluvial to lacustrine sequence comprises primarily micritic dolomite and clay minerals with occasional silt size quartz grains and silcrete fragments. Fe-oxide gravels of pisoliths and banded iron formation (BIF) fragments are also present, grading from <10% content just above the conglomerate to <1% in the upper core. Below 8 m depth, the detrital host sediments comprise a basal intraformational conglomerate of fragmented, reworked and recemented oxidised BIF infilled with some detrital sediments and dolomite cement, overlying a sharp contact to intact BIF at 10.7 m.

The detrital host sediments overlying the shale units within cores 009 and 015 are comparatively deeper (~14 to 16 m thick) and more heterogeneous. Bore cores 009 and 015 contain a basal white clay horizon of ~4 m thick that overlies in-situ regolith and saprolite. The uppermost alluvial sediments (overlying the white clay horizon) are distinct between the profiles, however, and are typically composed of clay-rich matrix and varying proportions of Fe-gravel and pisoliths (~1 mm to 5 cm), quartz grains and some relict silt size clay aggregates. Core 015 contains a fining up sequence consisting of ~50% pisolitic gravel (~1-5 mm diameter) at the base of the succession (~10.3 m depth) to <10% gravel within the top 3 m (Figure 5). The matrix within this sequence contains sub-millimetre pores, which appear to be from leaching and loss of grains. Overall, core 015 contains generally higher proportions of relict host

sediment and dolocretization was more heterogeneous; almost no dolomite occurs between 9 m and 10.3 m depth towards the base of the alluvial succession.

The upper section of core 009 (<5.7 m depth) contains ~10 to 40% magnetic pisolitic and platey gravel, typical of surface lags, within a matrix of clay to silt alluvium. Core 009 also contains a fining up sequence grading from ~10% gravel within the lower alluvial sequence (~8 to 12.7 m depth) to <1% gravel between 5.7 m to 8 m depth, where sediments are dominated by clay and also contain infrequent silcrete fragments. The coarse fraction with the lower alluvium is variable and consists of Fe-oxide cemented nodules and extraformational fragments of chert and weathered shale.

The basal pale to white clay-rich horizon in cores 009 (12.7-16.3 m) and 015 (10.3-14.1 m) is comprised of kaolinite, Fe-oxides and authigenic palygorskite, smectite and dolomite with fragments of silcrete (~1 to 10 cm). Coarse weathered shale clasts (~5-20 cm length) occur towards the base. The white clay horizon is typical of CzD2 sediments where locally derived from weathering of shale units (Kneeshaw and Morris, 2014). Underlying regolith contains higher proportions of kaolinite, quartz, mica and Fe-oxides from weathering of shale bedrock but still contains significant dolomite (~20 to 60 wt%). Intraformational lithic fragments of chert and shale increase with depth within the saprolite and saprock of cores 009 and 015. Intact shale bedrock is present below ~20 m depth. Dolomite content decreases within the saprolite, becoming more common as infill along fractures.

Mineralogy

The mineralogy of the dolocrete is mostly composed of dolomite (~50 to 95 wt%), with varying proportions of palygorskite, kaolinite, smectite, hematite, goethite, quartz, calcite (Figure 5), with mica and sepiolite occurring only in some cores. Two phases

of dolomite were identified from XRD patterns in most samples: (i) stoichiometric dolomite with 50 to 53 Mol% $CaCO_3$ (up to 82 wt%) and; (ii) Ca-rich dolomite with 53 to 60 Mol% $CaCO_3$ (typically <20 wt%, although a few samples contained up to 63 wt%). Both dolomite phases appear to be relatively well-ordered, as 015 and 021 reflections are visible in XRD patterns, although this is difficult to confirm in mixed samples with low Ca-dolomite proportions (Goldsmith and Graf, 1958; Drits et al., 2005). Calcite occurs primarily within a few metres of the surface and is secondary to dolomite. Calcite content ranges from 2-60 wt%, but is mostly <30 wt% and only exceeds dolomite content in one sample. Substitution of Mg in calcite ranges from 1.0 to 6.3 Mol% $MgCO_3$, but is mostly <5 Mol% $MgCO_3$. Minor amounts of magnesite (<1 to 6%) were also detected within three samples from the top 5 m of core 015. Mg-bearing clays (predominantly palygorskite and smectite) are common throughout the profiles and frequently comprise >10% of the mineral assemblage. Minor sepiolite was detected within the upper profiles of cores 010 and 015 (<5 wt% of bulk samples). Clay mineralogy is described in more detail below (in *Clay mineral associations and evidence of microbial structures*). The Fe-oxides, kaolinite, quartz, mica and some smectite minerals correspond to host sediment mineral composition and account for <35 wt% of the mineral assemblage within the main dolocrete profiles. Mica occurs only within the lower profiles of cores 009 and 015, in association with lithic fragments and shale bedrock.

Dolocrete characteristics and micromorphology

Dolocrete textures were largely controlled by host sediment texture and composition. Pedogenic carbonate nodules, composed of sub-micron clusters of Mg-calcite (6.3 Mol% $MgCO_3$) and dolomite, are present within a thin soil zone observed within the top 0.5 m of core 015 (Figure 6A). Below the soil zone, replacement and cementation by dolomite is strongly developed. Dolomite textures vary from planar-e to non-planar (Sibley and Gregg, 1987); no evidence of a calcite precursor was observed. Dolomite preferentially replaced finer clay sediments, and micritic dolomite (<10 µm; Figure 7B) - sometimes containing small proportions of clay or detrital remnants (Figure 7A) - has largely replaced the host sediment matrix throughout the profiles. Coarser dolomite textures were less frequent and typically present as a unimodal matrix of ~50-70 µm crystals. Replacement of coarser silt or clay aggregates by dolomite of ~50-100 µm crystals was also observed, typically within a micritic matrix.

Resistant grains, such as pisolitic gravel, lithic fragments and quartz, are not replaced but are frequently brecciated, as are many clay aggregates and weathered bedrock fragments (Figures 6C and F). Some quartz grains display dissolution features around the edges and are coated by clays or carbonate. Elongate fissures typically <1 mm diameter are common and cross-cut the matrix and void space surrounding resistant grains (Figure 6C); fissuring appears to be associated with shrinkage of the matrix from desiccation, as well as brecciation and volume change during dolocretization. No fossils or textural features indicative of lacustrine deposition, such as laminations, were observed.

Dolomite cements include both vadose gravitational cement (forming irregular lining of void walls and often not filling entire pores; Freytet, 1973) and uniform dolomite of

~20-70 µm diameter coating clasts and infilling pores, typical of phreatic cement (Figure 6B; Tucker, 1991). Phreatic cement also occurs as infill along preferential planes of coarse fractures and within macro-pores, including within the gravelly sediments of core 015 (Figure 6D). In general, the dolocrete matrix is highly cemented throughout the profiles. Larger voids more frequently remain open in the top ~5 m of core 009 and throughout the detrital sediments in cores 015 and 010; open voids frequently contain pore lining cements. The upper few metres of core 010 also contains overgrowth dolomite cements forming the outer zone of dolomite rhombs (Figure 7A). The later stage cements may correspond to the Ca-rich dolomite of 47-60 wt% detected by XRD within the top 3 m of this core (Figure 5).

Intracrystalline porosity is also observed in all cores, most frequently from dissolution of zones or cores (Figure 7C and E). The dissolution features are heterogeneous and not continuous throughout cores or even within samples. Hollow dolomite from dissolution of dolomite zones is particularly notable in the regolith of core 009 at ~12.7 m depth (Figure 7C). Core 010 contains irregular to rounded dolomite that appears to comprise multiple smaller dolomite crystals; intracrystalline porosity is present between these nano-crystals (Figure 7A).

Brecciation and cementation is common throughout all profiles and is particularly extensive within the middle to lower profiles of cores 009 (>5.7 m depth) and 015 (>10.3 m depth), which also contain high proportions of authigenic clay extending down to saprolite (Figure 5). Numerous curved fissures form a nodular structure within much of the sediments, and are often infilled by later dolomite. Dolocrete within the white clay horizon (cores 009 and 015; Figure 4) contains laminar cement that is frequently fragmented and re-cemented (Figure 6E and 6F).

Shale saprock textures are distinct from overlying dolocrete, characterised by more features of shale bedrock. Dolomite is still the dominant mineral in the saprock, followed by kaolinite in core 009 and goethite in core 015. The saprock is typically fractured. Multiple generations of dolomite are observed in the saprock zone of core 009 (Figure 6G), including planar-s matrix of crystals <100 µm, and Fe-stained non-planar spheroidal dolomite matrix (~10 to 300 µm) cross-cut by Fe-stained fan-shaped wedges of spheroidal dolomite within curvilinear structures of ~1-5 mm thickness (Figure 6H and Figure 7D). The spheroidal and fan-shaped dolomite has concentric zoning, although a radial structure is observed and is strongly developed within shale bedrock at ~20 m, suggesting a primary origin. Relict kaolin laths and occasional quartz grains occur within the dolomite. Petrographic relationships indicate Fe-oxide precipitation after the spheroidal dolomite. Later generations of dolomite are evident as non-stained laminar cement within fissures, in addition to inward coarsening void infill. The fissures appear to be shrinkage cracks from roots and or burrows and cross-cut the earlier formed Fe-stained dolomite. The dolomite within the core 015 saprock is present as coarse laminar cement and also as fragments of partly dissolved dolomite of <1 to ~20 µm diameter.

Clay mineral associations and evidence of microbial structures

Textural relationships indicated that dioctahedral smectite clays, although primarily authigenic, largely formed prior to dolocretization within the weathering profile. Smectite is dominant in core 015 where it comprises up to 30% of the mineral assemblage, although is typically ≤17% throughout all profiles, Smectite occurs as both replacement of matrix or discrete grains as well as pore infill. In contrast, palygorskite-sepiolite and some incipient smectites are closely associated with dolomite and microbial EPS structures. These Mg-bearing clays are syngenetic or

secondary to dolomite and are commonly interwoven around dolomite crystals, resembling microbial EPS (Figure 7E-H). Fossilised honeycomb structures and organic filaments are clearly observed, occurring in all cores and at various depths throughout the profiles. Fibrous palygorskite is most common, coating dolomite crystals and filling voids (Figure 7G and H), but does not fill dolomite intracrystalline pores (Figure 7C and E). Palygorskite is also observed replacing earlier clay aggregates. Palygorskite is particularly prevalent in core 009 where interwoven palygorskite-dolomite textures are common throughout the middle and lower profile, extending into saprolite (5.7 to 17 m depth; average 27 wt% palygorskite). Cores 010 and 015 contain comparatively less palygorskite, <5% and <15% respectively; however, palygorskite is most prominent in the top 2.5 m of core 010 and between ~12 to 13.5 m depth in core 015 (where palygorskite occurs within a clay-rich horizon overlying saprolite).

Calcretization

Secondary calcite cement and replacement of dolomite (dedolomitization) is observed within the top metre of all core profiles. The calcretization is most developed within the top 3 m of core 009, where calcite comprises up to 60 wt% at 0.8 m depth. Calcite infilled many fractures and voids surrounding pisoliths or detrital clasts (Figure 8A, B and D) and finer fractures cross-cutting the matrix, in addition to replacing the dolomite matrix (Figs 8A and C). Calcite within the matrix is largely micritic with non-planar contacts. Orientated calcite crystals commonly line void walls. These crystals are generally coarser in size at void walls (~100 µm length), and decrease in size towards micritic within void centres (Figure 7B). Dedolomitization is observed in the uppermost sample of core 009, whereas at 2.6 m, calcite occurs only as late stage cement and dolomite replacement features are not observed (Figure 8D). Low-Mg calcite (3.2

Mol% $MgCO_3$) and Ca-rich dolomite (57Mol% $CaCO_3$) occur within fine clayey sediments at ~10.4 m depth, immediately below the more permeable gravelly alluvial deposit within core 015.

Stable isotope geochemistry

Stable carbon and oxygen isotope compositions of dolomite exhibit a positive covariance and significant correlation between $\delta^{18}O$ and $\delta^{13}C$ values (R^2 = 0.25; p=<0.0001; Figure 9). Dolomite $\delta^{18}O$ values range from -7.63 to -3.40‰ (median -5.88‰); however, the majority of $\delta^{18}O$ values are within the narrow interquartile range of -6.20 to -5.34‰. The $\delta^{13}C$ values of dolomite are mostly within a narrow range of -6.27 to -4.28 ‰ (median -5.43‰). Two higher $\delta^{13}C$ values of -3.90‰ and -3.52‰ occur within core 015; the first, a late stage cement within a gravelly host sediment dominated zone at 6.5 m depth, and the latter associated with pedogenic carbonate at 0.3 m depth.

Overall, $\delta^{13}C$ and $\delta^{18}O$ values do not show systematic trends with depth, although there are variations within profiles. The $\delta^{13}C$ and $\delta^{18}O$ values of core 010 are slightly more variable in the upper profile (<5.7 m). In particular, the top 3 m of core 010 (containing higher proportions of Ca-dolomite) has $\delta^{18}O$ values of -5.35 to -3.58 ‰. The $\delta^{13}C$ values in core 009 are within a narrow range; $\delta^{13}C$ decreases with depth before increasing below 16 m in the lower saprolite and saprock. The $\delta^{13}C$ values within core 015 do not display clear trends with depth and mostly range between -6.0 and -4.74‰, with slightly higher values of ~-5.10 to -4.74 ‰ within the saprock. The $\delta^{18}O$ values in cores 009 and 015 also display a similar pattern of higher $\delta^{18}O$ values of -4.95 to -3.40 ‰ within shale saprock at >18 m depth. The $\delta^{18}O$ values of -3.85 to -3.40‰ correspond to pale peach to grey coloured infill of fractures. The $\delta^{18}O$ values

in core 015 range from -7.22 to -3.84 ‰, and are more variable below the change in host sediment at 10.3 m (where the Ca-dolomite sample at 10.45 m has a lower $\delta^{18}O$ value of -7.22‰).

Calcite $\delta^{13}C$ values are variable and range from -6.69 to -3.42‰; $\delta^{18}O$ values range from -8.36 to -4.35‰ (Figure 9). The calcite $\delta^{13}C$ and $\delta^{18}O$ values are distinct between two shallow samples from core 015, associated with pedogenic carbonate, and calcite cement and matrix from core 009 and 015. Calcite in non-pedogenic samples has a notably lower range of $\delta^{18}O$ values (-8.36 to -7.45‰) and $\delta^{13}C$ values are similar to dolomite, ranging from -6.69 to -4.39‰. A lower calcite $\delta^{18}O$ value of -8.14‰ in core 015 at 10.35 m corresponds to the low $\delta^{18}O$ composition of Ca-dolomite at a similar depth. In contrast, samples from the pedogenic zone in core 015 have relatively higher calcite $\delta^{13}C$ and $\delta^{18}O$ values; a bulk sample containing mixed carbonate matrix and pedogenic nodules has a $\delta^{13}C$ value of -4.47‰ and $\delta^{18}O$ value of -6.20‰, while a sub-sample of white carbonate next to plant root material has a higher $\delta^{13}C$ value of -3.42‰ and $\delta^{18}O$ value of-4.35‰.

Discussion

This study demonstrates that groundwater dolocrete formed within an evaporitic sub-basin within the Hamersley Ranges. The distribution and characteristics of dolocrete support the existence of isolated sub-basins across the region, under arid conditions (as suggested by Kneeshaw and Morris, 2014); high evaporation from shallow groundwater systems is presumed to have promoted carbonate precipitation in the Late Miocene-Pliocene. Our approach, using combined mineralogical, micromorphological and stable carbon and oxygen isotope analyses of dolocrete samples, provides the first evidence of the hydrochemistry of groundwater during this

period of dolocrete formation. Our results also show that primary dolomite precipitated from relatively saline groundwater and that microbial EPS was important for providing nucleation sites. These findings suggest that microbial activity may be important for dolocrete formation in other groundwater environments.

Groundwater origin of Coondiner dolocrete

The Coondiner dolocretes contain numerous features characteristic of groundwater calcretes and dolocretes, and are similar to those described in other semi-arid to arid drainage basins worldwide (Mann and Horwitz, 1979; Khalaf, 1990; El-Sayed et al., 1991; Spötl and Wright, 1992; Nash and McLaren, 2003). The multi-metre thickness of the profiles, presence of phreatic cements and lack of root traces are all suggestive of groundwater formation (Spötl and Wright, 1992). The pervasive replacement of host sediments by dominantly uniform dolomite (<100 um) matrix is also characteristic of massive groundwater dolocrete profiles (Spötl and Wright, 1992), and is distinct from discrete pedogenic dolocrete nodules formed at the top of profiles. The Coondiner dolocretes developed primarily within non-carbonate host sediments dominated by kaolinite and Fe-oxides, and cemented both detrital sediments and regolith down to bedrock. No biogenic or textural features indicative of lacustrine dolomite were observed, although predominantly micritic dolomite largely devoid of detrital host sediments in the upper profile of core 010 could reflect lacustrine deposition. The abundance of authigenic Mg-clays is characteristic of many dolocrete profiles worldwide, indicative of the Mg-rich environment (Colson et al., 1998; Kadir et al., 2010; Wanas and Sallam, 2016). Dissolution of silicates within the host sediment appears to have promoted clay formation as fluids became increasingly Si-rich during dolocretization. Brecciation and cementation of resistant grains and aggregates

observed throughout the profiles is also typical of the displacive growth of groundwater dolocretes (Mann and Horwitz, 1979; Wright and Tucker, 1991).

The presence of Fe-stained spheroidal dolomite within saprock appears to reflect an earlier phase of dolomite precipitation within a different depositional setting. The concentric zoned, radial cements and spheroids of Fe-stained dolomite within shale saprock were distinct from overlying dolocrete, and were similar to zebraic dolomite cements described by Simonson et al. (1993) associated with seafloor precipitation within the Hamersley Basin. The different environmental setting is also indicated by higher $\delta^{18}O$ values of >-4‰ within saprock dolomite. The $\delta^{18}O$ values of marine carbonate would usually be ~-2 to +2‰. It is possible, however, that overprinting of dolocretization on saprock has occurred; it is also challenging to extract pure sub-samples for stable isotope analysis. The petrographic relationships and secondary Fe-oxides around the spheroids confirm the earlier timing of formation. Extensive shrinkage cracks and fissures within the saprock subsequent to spheroidal textures appear to have formed from root cracks or burrows, and indicate that the bedrock was once close to or at the surface (and hence influenced by intensive bioturbation) prior to the deposition of overlying transported sediments. The later stage, non-stained dolomite cements within saprock are interpreted to have formed as part of the Cenozoic dolocretization event.

Environmental controls on dolocrete formation

Existing models of groundwater dolocrete formation cannot fully explain the distribution of dolocrete within the Hamersley Ranges. The occurrence of groundwater dolocrete in the upper reaches of the Coondiner catchment (in addition to dolocrete outcrops at Weeli Wolli Creek etc.) is in contrast to the majority of documented

groundwater dolocrete sequences – these are generally found in evaporitic settings at the terminus of major (palaeo)drainage systems, downgradient of groundwater calcrete and upgradient of gypcrete and possibly halite (Arakel, 1986; Spötl and Wright, 1992; Armenteros et al., 1995). Whilst dolocrete has been identified in the terminal Fortescue Marsh (Mather et al., 2018), the extensive dolocrete duricrusts documented here, in a sub-basin in a regional upland setting, do not appear connected to calcrete or gypcrete facies, although they are distributed in localised topographic lows. Erosion largely ongoing since the Pliocene has lowered regional base level and resulted in dissection of the Coondiner dolocrete. Thus, the full distribution of Cenozoic duricrusts may not be represented within the modern landscape. However, the shallow gradient in topography, depth to bedrock and groundwater level along the Coondiner sub-basin strike valley connecting to the Coondiner dolocrete would suggest that associated duricrusts would still be represented within the valley sediments. We might also expect to observe outcrops remnant duricrust along valley flanks if cemented calcrete or dolocrete had occurred throughout the valley. Where present, the carbonate duricrust within the strike valley is dolocrete, although a pre-cursor calcrete cannot be discounted. The heterogeneous and patchy distribution of dolocrete within the Coondiner sub-basin strike valley suggests dolocretization occurred in localised depressions but that the main locus of dolocretization was focussed in the area of groundwater emergence where the Coondiner dolocrete is now mostly exposed at the surface. An alternate model of groundwater dolocrete formation was proposed by Colson and Cojan (1996), who described numerous dolocretes within the Provence Basin, France. These dolocretes were labelled “halo dolocrete”, and formed around palaeo-playas where mixing between regional groundwaters and lake brines was vital for driving dolomite precipitation. In contrast, the distribution of dolocretes in the

Hamersley Ranges largely extends throughout the detrital and regolith sediments, constrained by banded iron formation ridges, and does not appear to follow a halo pattern. This suggests that other environmental conditions were important for dolocrete formation.

The results obtained from the Coondiner dolocrete profiles indicate that the palaeoenvironmental conditions and palaeogeography of the sub-basin were different from the modern setting, and can explain the distribution of dolocrete in similar contexts. Mineralogical and stable oxygen isotope data indicate that the dolocrete developed in a saline-evaporitic setting. Chemical sedimentation was strongly developed, whereby authigenic carbonates and Mg-clay comprised 85-100% of the mineral assemblage throughout much of the profiles. Dolomite and palygorskite are most commonly associated with semi-arid to arid environments (Singer and Galan, 1984; Arakel, 1986; Armenteros et al., 1995; Colson et al., 1998), influenced by periodic wetting and desiccation cycles (Calvo et al., 1999; Deelman, 2003). Abundant shrinkage cracks, laminar dolomite cements within solution pipes and voids (Arakel and McConchie, 1982), and the presence of both phreatic and gravitational cements throughout profiles, also indicate a fluctuating water table (cf. Nash and McLaren, 2003). The stable oxygen isotope compositions of dolomite reflect the groundwater hydrochemical conditions in which the mineral precipitated, and in particular the degree of evaporation and thus salinity (which is strongly correlated with $\delta^{18}O$; Dogramaci et al., 2012; Skrzypek et al., 2013). The Coondiner dolocrete $\delta^{18}O$ values overlap with Cenozoic groundwater dolocrete formed within the Fortescue Marsh (Figure 9; Mather et al., 2018). Mather et al., (2018) estimated palaeogroundwater chemistry from which dolomite precipitated by: 1) modelling the palaeogroundwater $\delta^{18}O$ values (from dolomite $\delta^{18}O$ values) over a probable range of temperatures using

the equation for low temperature dolomite-water fractionation by Vasconcelos et al., (2005) assuming dolomite precipitation in isotopic equilibrium with solution $\delta^{18}O$; and 2) calculation of salinity using a linear regression model between groundwater $\delta^{18}O$ and salinity in total dissolved solids (TDS). Mather et al., (2018) determined that the Fortescue Marsh contained two groups of dolocrete; (i) deeper dolocrete (G1) formed from highly saline to brine groundwater (estimated TDS of 79-150 g/L at average groundwater temperature of 30°C) and; (ii) shallower (G2) dolocrete formed from brackish to saline groundwater (estimated TDS of 33-46 g/L at 30^{o}C). The majority of the Coondiner dolomite exhibits $\delta^{18}O$ compositions overlapping or higher than those for the Fortescue Marsh G2 dolocrete but mostly lower than the G1 dolocrete (Figure 9), suggesting precipitation of the Coondiner dolomite from brackish to highly saline groundwater (Mather et al., 2018). This inferred groundwater chemistry is in contrast to modern groundwater, which is notably fresh, and indicates that the palaeo-sub-basin was disconnected from Coondiner Creek drainage and was hydrologically closed; this would have allowed the build-up of salts in groundwater from evapoconcentration. The statistically significant correlation between dolomite $\delta^{18}O$ and $\delta^{13}C$ values is also indicative of a hydrologically closed system (Spötl and Wright, 1992; Arenas et al., 1997), although the correlation was relatively weak (R^2 = 0.25; p=<0.0001). Variability in $\delta^{18}O$ and $\delta^{13}C$ values may, therefore, reflect both variation in recharge and evaporation conditions as well as broader shifts in hydroclimatic conditions. The distribution of the Coondiner dolocrete may be further explained by underlying impermeable bedrock, which would result in shallow ponding of groundwater in periods of no or highly restricted outflow. A past saline-evaporitic setting supports the hypothesis put forward by Kneeshaw and Morris (2014) that the

sub-basins where extensive carbonates (such as the Oakover lacustrine limestone and calcrete) have formed were previously isolated, due to damming of valleys.

Regional groundwater chemistry was crucial for dolocrete formation. The Mg-Ca-HCO_3 type composition of groundwater provided the source of ions for subsequent dolomite precipitation. In effect, dolocrete development represents a redistribution of ions from the Proterozoic marine dolomite of the Wittenoom Formation. Importantly, the pCO_2 of groundwater within the Wittenoom Formation aquifer and alluvial aquifer in the study area is an order of magnitude or more greater than atmospheric pCO_2 (pCO_2(WF) = 0.03631 atm; pCO_2(SA) = 0.05129 atm; pCO_2(air) = 0.00039 atm; calculated using PHREEQC geochemical modelling software by Parkhurst, 1980; Table S1). Therefore, outgassing of CO_2 occurs near the surface, as shallow groundwater begins to equilibrate with surface pressures, increasing the pH and CO_3^{2-} activity and promoting dolomite precipitation. Higher than expected $\delta^{13}C$ values of dolomite may reflect increasing $\delta^{13}C$ in dissolved inorganic carbon (DIC) of source groundwater during CO_2 degassing (Jacobson et al., 1988; Talbot, 1990). The relatively narrow range of $\delta^{13}C$ values of dolomite in this study suggests a similar composition of DIC in groundwater over time, and is likely due to the fairly constant source of DIC from the Wittenoom Formation aquifer (Dogramaci and Skrzypek, 2015; Mather et al., 2018; McCallum et al., 2018). In addition, the majority (>95%) of the $\delta^{13}C$ values of dolomite fall within the same range as the Fortescue Marsh dolocretes, indicating that DIC is similar across the catchment. Based on the expected fractionation between HCO_3 in groundwater DIC and dolomite ($\Delta^{13}C_{HCO3\text{-}dol}$ = 3.5-3.7‰ at 20-30^{o}C; Deines et al., 1974; Mook et al., 1974; Golyshev et al., 1981), the dolomite precipitated from groundwater with $\delta^{13}C$ values between –9.9 and -7.1‰. This range partly overlaps with measured DIC of local groundwater (-11.40 to -9.05 ‰; Table S1),

but also suggests that the majority of dolomite precipitated from waters with slightly higher DIC $\delta^{13}C$.

Origin of dolomite

A primary or early diagenetic origin of dolomite is indicated by the lack of a carbonate-precursor observed within Coondiner samples. Primary or early diagenetic dolomite has been frequently observed in other massive groundwater dolocretes (Arakel, 1986; Khalaf, 1990; El-Sayed et al., 1991; Spötl and Wright, 1992; Casado et al., 2014) including within the Fortescue Marsh (Mather et al., 2018). The presence of both stoichiometric and Ca-rich dolomite in the dolocrete profiles indicates at least two phases of dolomite precipitation. Variation in Ca content in dolomite may reflect changes in Mg/Ca ratios in solution during formation. However, primary dolomite generally forms as a poorly ordered Ca-rich dolomite, which stabilises to well-ordered stoichiometric dolomite over time (Morrow, 1982; Alonso-Zarza and Martín-Pérez, 2008; Bontognali et al., 2014a). This suggests that Ca-rich dolomite may represent younger dolomite, yet to fully undergo diagenetic stabilisation. The loss of Ca-rich zones over time may also be reflected by hollow cores and zones of dolomite crystals observed throughout the profiles. Dolomite $\delta^{18}O$ and $\delta^{13}C$ values did not show any obvious trends with depth or Ca-dolomite vs stoichiometric dolomite content. However, slightly higher $\delta^{18}O$ values in the upper profile of core 010 dominated by Ca-rich dolomite, may suggest a phase of Ca-dolomite formation under higher evaporation rates. In contrast, a lower $\delta^{18}O$ value of -7.22‰ of Ca-dolomite occurring below the gravelly alluvial deposit in core 015 suggests precipitation from fresher water, and is likely associated with preferential flow of water through the zone of high permeability; there may also be perched water overlying the more clay-rich regolith below.

Whilst the palaeo-hydrochemical conditions were conducive to dolomite formation, the presence of microbial EPS may explain the primary origin of dolomite, providing nucleation sites to overcome the kinetic barriers of dolomite precipitation. Petrographic observations indicated that EPS influenced both dolomite and clay authigenesis at the study site (Figs 6E-H). Honeycomb structures and filaments connecting around dolomite crystals (Figs 6E-H) are characteristic of EPS morphologies observed in saline evaporitic environments elsewhere (Bontognali et al., 2010; Spadafora et al., 2010; Petrash et al., 2017). The presence of Mg-clays connecting and replacing with EPS structures surrounding the dolomite suggests the clay formation was also promoted by EPS and was closely related to dolomite precipitation. The lack of clay within partly dissolved dolomite crystals further demonstrates the close timing of clay and dolomite precipitation. Microbial influence upon clay authigenesis has not been as fully explored. However, Bontognali et al. (2014b) demonstrated microbial mineralisation of smectite in laboratory experiments, while others (e.g. Casado et al., 2014; Wanas and Sallam, 2016) have suggested that incipient Mg-clay formation may be important for dolomite precipitation, with early viscous clay material further promoting nucleation.

The presence of EPS throughout the Coondiner dolocrete profiles is indicative of high microbial activity in the past. However, it is not certain whether active microbial respiration was a driver of precipitation, since there is no clear stable isotope indication of sulphate-reduction (such as lower $\delta^{13}C$ values; Petrash et al., 2017). Due to various influences on isotope signatures, identifying a microbial influence can be challenging and stable oxygen and carbon isotope signatures have been found to be similar regardless of biotic vs. abiotic processes (Casado et al., 2014; Petrash et al., 2017). Regardless, the textural association of dolomite and Mg-clay with EPS suggests the

two are intrinsically linked and that microbial EPS was important for nucleation of the minerals. Previous studies that describe dolocrete within the Hamersley Basin (e.g. Barnett and Commander, 1985; Mather et al., 2018) do not investigate the potential role of microbial influence and therefore, do not include the detail of petrographic observations where such features may be observed. However, the presence of associated EPS and clay minerals within the Coondiner dolocrete raises the possibility that these factors may have played a role in groundwater dolocrete formation regionally.

Surface alteration of dolocrete

Various geomorphic processes have altered the dolocrete since its formation, including erosion of the dolocrete surface and dissection by more recent drainage. Evidence of pedogenic processes is minimal, and only a thin horizon of pedogenic carbonate containing calcite with distinct $\delta^{13}C$ and $\delta^{18}O$ compositions has developed. The relatively higher $\delta^{13}C$ and $\delta^{18}O$ values of calcite in the pedogenic zone may reflect higher evaporation rates within the soil profile. Surprisingly, $\delta^{13}C$ values are not lower in the soil zone as might be expected in pedogenic carbonate. Calcretization of the dolocrete has extended deeper, occurring within the top ~4 m and in deeper zones of higher permeability (e.g. at the base of a gravelly flood deposit at 10.3 m where water likely becomes perched over clayey sediments below). However, calcretization was only minor and calcite proportions only exceed dolomite within the top 0.5 m. The lower range of calcite $\delta^{18}O$ values and presence of gravitational cements suggests calcite precipitation from relatively fresher meteoric waters in the vadose zone (Armenteros, 2010), a feature characteristic of dolocrete exposed to vadose processes (Khalaf and Abdal, 1993; Arenas et al., 1999). Coarse cement lining pores indicates prolonged periods of wetting allowing larger crystals to form, and the inward fining of crystals may

reflect drying following pore occlusion. Whilst the majority of calcite appears to be present as pore-filling cement, replacement of dolomite by calcite (dedolomitization) can be observed within the most calcite-rich sediments. Undersaturation of dolomite within infiltrating meteoric waters may promote dissolution of dolomite, particularly less stable Ca-rich dolomite. Dissolution of gypsum is also a common driver of dedolomitization, as the release of Ca and SO_4 both promote dolomite dissolution and precipitation of calcite (Sanz-Rubio et al., 2001; Jin et al., 2010). However, within the Coondiner dolocrete, lack of textural evidence of earlier gypsum combined with limited calcretization suggests gypsum dissolution has not been a major driver of dedolomitization. The $\delta^{13}C$ values of secondary calcite (pedogenic and groundwater) indicate precipitation from groundwater with higher DIC $\delta^{13}C$ (palaeogroundwater $\delta^{13}C$ = -8.6 to -5.4‰ calculated from$\Delta^{13}C_{HCO3\text{-}cal}$ = 1.9-2.0‰ at 20-30^{o}C; Deines et al., 1974; Mook et al., 1974; Golyshev et al., 1981) compared to measured groundwater $\delta^{13}C$ signatures (-11.40 to -9.05 ‰; Table S1); this suggests CO_2 degassing may also be a driver of calcite precipitation within the shallow sediments.

Model for groundwater dolocrete formation

Based on the new information obtained from the Coondiner dolocrete profiles, a model for groundwater dolocrete formation and development in the landscape can be proposed (Figure 10). The first stage in the process (Figure 10A) required the development of a shallow groundwater system under semi-arid to arid conditions that were conducive to carbonate precipitation. Damming of valleys occurred during the Miocene, caused by deposition of large volumes of predominantly clay sediments of CzD2 (Morris and Ramanaidou, 2007). This resulted in hydrologically closed sub-basins that allowed groundwater chemistry to evolve to promote carbonate formation. The second (Figure 10B) involved the initial development of dolocrete (Figure 10B).

Dolomite precipitation was promoted by evaporitic conditions combined with high Mg/Ca ratios and increased CO_3^{2-}/HCO_3^- ratios in groundwater (Petrash et al., 2017). These hydrochemical conditions occurred due to (i) regionally elevated Mg concentrations within groundwater from weathering of the dolomitic Wittenoom Formation, (ii) increased salinity (concentration of ions) and pH as shallow groundwater underwent evaporation within an internally draining basin, and (iii) increased CO_3^{2-} activity relative to HCO_3^- in groundwater due to CO_2 degassing from emerging waters, as high pCO_2 of groundwater equilibrated with surface pressures. Stage three (Figure 10C) involved the continued and displacive growth of dolocrete. The dolocrete built outward and upward as dolomite continued to precipitate close to the water table and was constrained below by bedrock (similar to the process described for groundwater calcrete by Mann and Horwitz, 1979, pp. 298). Eventually the isolated 'pods' of dolocrete shown in Figures 10B and 10C developed into a larger body of dolocrete. The upward growth of dolocrete resulted in dolocrete being pushed up above the water table and towards the surface as shown in Figure 10D. Ongoing erosion since the Pliocene has exposed the dolocrete at the surface and led to its dissection by modern drainage (Figure 10E). A lower water table and outflow to Coondiner Creek has resulted in fresher groundwater and conditions that are no longer conducive to dolocrete formation. The influence of fresher meteoric water within the vadose zone also resulted in calcretization of the uppermost parts of the dolocrete profile.

Conclusions

This study has (i) provided the first detailed characterisation of groundwater dolocrete within a regionally elevated sub-basin in the Hamersley Basin geological province, and (ii) presented a new model for groundwater dolocrete formation. This model is distinct

from classic explanations of groundwater dolocrete development in terminal basin settings. Dolocretes within the Hamersley Basin are distributed within zones of shallow and emerging groundwater, controlled by both geomorphic and hydrogeologic factors associated with the ridge and valley terrain. Dolocrete formation was promoted by the regional presence of Mg-rich groundwater under evaporitic palaeoenvironmental conditions within internally draining sub-basins, most likely during the Late Miocene and Pliocene (Kneeshaw and Morris, 2014). In these settings, evaporation and CO_2 degassing (increasing pH) from shallow Mg-rich groundwater appear to have been the major drivers of dolocrete development, without a requirement for significant down-dip hydrochemical modification. The formation of dolocrete under more saline-evaporitic conditions is supported by the dolomite $\delta^{18}O$ values, which overlap with $\delta^{18}O$ ranges of saline-formed Cenozoic dolocretes within Fortescue Marsh and suggest precipitation from brackish to highly saline groundwater (Mather et al., 2018). Higher than expected $\delta^{13}C$ values of dolomite may also reflect increasing $\delta^{13}C$ during CO_2 degassing. The distribution of large dolocrete outcrops, such as at Coondiner Creek, may be explained by ponding of shallow groundwater overlying relatively impermeable bedrock during periods of no or highly restricted outflow. The past evaporitic environment is in contrast to modern conditions, where groundwater is fresh due to a relatively lower water table and outflow to Coondiner Creek. The influence of fresher water and vadose processes in the modern setting has resulted in secondary calcrete development at the top of dolocrete profiles. However, there is no evidence of pre-cursor calcrete prior to dolocrete development.

Microbial EPS promoted dolomite and clay (smectite and palygorskite) authigenesis within the Coondiner dolocrete. Importantly, the EPS provided nucleation sites to overcome the kinetic barriers of dolomite precipitation. High microbial activity within

groundwater systems suggests that the presence of EPS may also be important for dolocrete formation in other locations worldwide. Thus far, investigation of the role of microbial EPS in dolomite precipitation has focussed lacustrine or shallow marine microbialite environments (e.g. Vasconcelos and McKenzie, 1997; Van Lith et al., 2002; Wacey et al., 2007; Spadafora et al., 2010; Bontognali et al., 2012). Groundwater dolocrete therefore, provides a new opportunity to study the function of microbial EPS in dolomite precipitation within a different environment. In particular, further work is needed to define the role of EPS in clay authigenesis and determine the association with dolomite.

The outcomes from this study suggest that dolocretes may be more widespread in landscapes than currently recognised. This is particularly true of regions with Mg-rich groundwater derived from weathering of Mg-rich rocks, including marine dolomite but also volcanic or other Mg-igneous lithologies (Hutton and Dixon, 1981; Alonso-Zarza et al., 2016). The prevalence of dolocretes in the Hamersley Basin is similar to the extensive valley and channel calcretes described within inland Australia. In these settings, any localised evaporitic depressions may result in the formation of thick dolocrete profiles. The distribution and chemistry of groundwater dolocrete, may therefore, provide an underutilised archive for paleoenvironmental conditions and landform evolution in many semi-arid and arid drainage basins worldwide.

Acknowledgements

This research was supported by Rio Tinto Iron Ore. Caroline Mather was personally supported by The University of Western Australia's (UWA) Robert and Maude Gledden Postgraduate Scholarship. The authors acknowledge the facilities and the scientific and technical assistance of the Australian Microscopy and Microanalysis Research

Facility at the Centre of Microscopy, Characterisation and Analysis, The University of Western Australia, a facility funded by the University, State and Commonwealth Governments. We would like to thank Wade Dodson, Paul Hedley, and Glenn Kirkpatrick from Rio Tinto for technical support and assistance in the field. We especially thank Paul MacIntyre (UWA) and Maree Swebb (Rio Tinto) for assistance with digital elevation and aerial photography figure preparation. We would also like to thank Crisogono Vasconcelos (ETH-Zurich) and Moyra Wilson from UWA for assistance with carbonate petrography. Finally, we are grateful to Douglas Ford and Ela Skrzypek at the West Australia Biogeochemistry Centre at UWA and Mark Raven at Mineralogical Services, CSIRO for assistance with sample analysis.

References

Alley, NF, Clarke, JDA, MacPhail, M, Truswell, EM. 1999. Sedimentary infillings and development of major Tertiary palaeodrainage systems of south-central Australia. In Thiry, M, Simon-Coincon, R. (eds). Palaeoweathering, palaeosurfaces and related continental deposits. Special Publication Number 27, International Association of Sedimentologists. Blackwell Science, Oxford, 337-366.

Alonso-Zarza, AM. 2003. Palaeoenvironmental significance of palustrine carbonates and calcretes in the geological record. Earth-Science Reviews 60(3): 261-298.

Alonso-Zarza, AM, Bustamante, L, Huerta, P, Rodríguez-Berriguete, Á, Huertas, MJ. 2016. Chabazite and dolomite formation in a dolocrete profile: An example of a complex alkaline paragenesis in Lanzarote, Canary Islands. Sedimentary Geology 337: 1-11.

Alonso-Zarza, AM, Martín-Pérez, A. 2008. Dolomite in caves: recent dolomite formation in oxic, non-sulphate environments. Castañar Cave, Spain. Sedimentary Geology 205(3): 160-164.

Arakel, AV. 1986. Evolution of calcrete in palaeodrainages of the Lake Napperby area, central Australia. Palaeogeography, Palaeoclimatology, Palaeoecology 54(1): 283-303.

Arakel, AV, McConchie, D. 1982. Classification and genesis of calcrete and gypsite lithofacies in paleodrainage systems of inland Australia and their relationship to carnotite mineralization. Journal of Sedimentary Research 52(4): 1149-1170.

Arenas, C, Casanova, J, Pardo, G. 1997. Stable-isotope characterization of the Miocene lacustrine systems of Los Monegros (Ebro Basin, Spain): palaeogeographic and palaeoclimatic implications. Palaeogeography, Palaeoclimatology, Palaeoecology 128: 133-155.

Arenas, C, Alonso-Zarza, AM, Pardo, G. 1999. Dedolomitization and other early diagenetic processes in Miocene lacustrine deposits, Ebro Basin (Spain). Sedimentary Geology 125(1): 23-45.

Armenteros, I. 2010. Diagenesis of carbonates in continental settings. In Alonso Zarza, A, Tanner, LH. (eds). Carbonates in Continental Settings: Geochemistry, Diagenesis and Applications: Elsevier, Amsterdam 62: 61-151.

Armenteros, I, Bustillo, MAA, Blanco, JA. 1995. Pedogenic and groundwater processes in a closed Miocene basin (northern Spain). Sedimentary Geology 99(1): 17-36.

Barnett, JC. 1980. Mesozoic and Cainozoic sediments in the western Fortescue Plain. Western Australian Geological Survey Annual Report 3542.

Barnett, JC, Commander, DP. 1985. Hydrogeology of the Western Fortescue Valley, Pilbara Region, Western Australia. Western Australia Geological Survey, Perth.

Bischoff, WD, Bishop, FC, Mackenzie, FT. 1983. Biogenically produced magnesian calcite; inhomogeneities in chemical and physical properties; comparison with synthetic phases. American Mineralogist 68(11-12): 1183-1188.

Bontognali, TRR, Vasconcelos, C, Warthmann, RJ, Bernasconi, SM, Dupraz, C, Strohmenger, CJ, McKenzie, JA. 2010. Dolomite formation within microbial mats in the coastal sabkha of Abu Dhabi (United Arab Emirates). Sedimentology 57(3): 824-844.

Bontognali, TRR, Vasconcelos, C, Warthmann, RJ, Lundberg, R, McKenzie, JA. 2012. Dolomite-mediating bacterium isolated from the sabkha of Abu Dhabi (UAE). Terra Nova 24(3): 248-254.

Bontognali, TRR, McKenzie, JA, Warthmann, RJ, Vasconcelos, C. 2014a. Microbially influenced formation of Mg-calcite and Ca-dolomite in the presence of exopolymeric substances produced by sulphate-reducing bacteria. Terra Nova 26(1) 72-77.

Bontognali, TRR, Martinez-Ruiz, F, McKenzie, JA, Bahniuk, A, Anjos, S, Vasconcelos, C. 2014b. Smectite synthesis at low temperature and neutral pH in the presence of succinic acid. Applied Clay Science 101: 553-557.

Bowler, JM. 1976. Aridity in Australia, Origins and Expression in Aeolian Landforms and Sediments. Earth Science Reviews 12: 279-310.

Brand, WA, Coplen, TB, Vogl, J, Rosner, M, Prohaska, T. 2014. Assessment of international reference materials for isotope-ratio analysis (IUPAC Technical Report). Pure and Applied Chemistry 86(3): 425-467.

Calvo, JP, Blanc-Valleron, MM, Rodríguez-Arandía, JP, Rouchy, JM, Sanz, ME. 1999. Authigenic clay minerals in continental evaporitic environments. International Association of Sedimentologists Special Publications 27: 129-151.

Carlisle, D. 1983. Concentration of uranium and vanadium in calcretes and gypcretes. Geological Society, London, Special Publications 11(1): 185-195.

Casado, AI, Alonso-Zarza, AM, La Iglesia, Á. 2014. Morphology and origin of dolomite in paleosols and lacustrine sequences. Examples from the Miocene of the Madrid Basin. Sedimentary Geology 312: 50-62.

Colson, J, Cojan, I. 1996. Groundwater dolocretes in a lake-marginal environment: an alternative model for dolocrete formation in continental settings (Danian of the Provence Basin, France). Sedimentology 43: 175-188.

Colson, J, Cojan, I, Thiry, M. 1998. A hydrogeological model for palygorskite formation in the Danian continental facies of the Provence Basin (France). Clay Minerals 33(2): 333-347.

Curtis, R, Evans, G, Kinsman, DJJ, Shearman, DJ. 1963. Association of dolomite and anhydrite in the recent sediments of the Persian Gulf. Nature 197(4969): 679-680.

Das Sharma, S, Patil, DJ, Gopalan, K. 2002. Temperature dependence of oxygen isotope fractionation of CO_2 from magnesite-phosphoric acid reaction. Geochimica et Cosmochimica Acta 66(4): 589-593.

Deelman, JC. 2003. Low-temperature formation of dolomite and magnesite, Compact disc publications, Eindhoven, The Netherlands.

Deines, P, Langmuir, D, Harmon, RS. 1974. Stable carbon isotope ratios and the existence of a gas phase in the evolution of carbonate ground waters. Geochimica et Cosmochimica Acta 38(7): 1147-1164.

Dogramaci, S, Skrzypek, G. 2015. Unravelling sources of solutes in groundwater of an ancient landscape in NW Australia using stable Sr, H and O isotopes. Chemical Geology 393-394: 67-78.

Dogramaci, S, Skrzypek, G, Dodson, W, Grierson, PF. 2012. Stable isotope and hydrochemical evolution of groundwater in the semi-arid Hamersley Basin of subtropical northwest Australia. Journal of Hydrology 475: 281-293.

El-Sayed, MI, Fairchild, IJ, Spiro, B, 1991. Kuwaiti dolocrete: petrology, geochemistry and groundwater origin. Sedimentary Geology 73(1): 59-75.

Eugster, HP. 1980. Geochemistry of evaporitic lacustrine deposits. Annual Review of Earth and Planetary Sciences 8: 35-63.

Fellman, JB, Dogramaci, S, Skrzypek, G, Dodson, W, Grierson, PF. 2011. Hydrologic control of dissolved organic matter biogeochemistry in pools of a subtropical dryland river. Water resources research 47(6): 1-13. DOI: 10.1029/2010WR010275.

Freytet, P. 1973. Petrography and paleo-environment of continental carbonate deposits with particular reference to the Upper Cretaceous and Lower Eocene of Languedoc (Southern France). Sedimentary Geology 10:25-60.

Golyshev, SI, Padalko, NL, Pechenkin, SA. 1981. Fractionation of stable isotopes of carbon and oxygen in carbonate systems. Geochemistry International 18(5): 85-99.

Goudie, A. 1972. The chemistry of world calcrete deposits. The Journal of Geology 80(4): 449-463.

Griebler, C, Lueders, T. 2009. Microbial biodiversity in groundwater ecosystems. Freshwater Biology 54: 649-677.

Haest, M, Cudahy, T, Laukamp, C, Gregory, S. 2012. Quantitative Mineralogy from Infrared Spectroscopic Data. II. Three-Dimensional Mineralogical Characterization of the Rocklea Channel Iron Deposit, Western Australia. Economic Geology 107: 229-249.

Heim, JA, Vasconcelos, PM, Shuster, DL, Farley, KA, Broadbent, G. 2006. Dating paleochannel iron ore by (U-Th)/He analysis of supergene goethite, Hamersley province, Australia. Geology 34(4): 173-176.

Hewson, RD, Cudahy, TJ, Drake-Brockman, J, Meyers, J, Hashemi, A. 2006. Mapping geology associated with manganese mineralisation using spectral sensing techniques at Woodie Woodie, East Pilbara. Exploration Geophysics 37: 389-400.

Humphreys, WF. 2001. Groundwater calcrete aquifers in the Australian arid zone: the context to an unfolding plethora of stygal biodiversity: Records of the Western Australian Museum, Supplement 64: 63-83.

Hutton, JT, Dixon, JC. 1981. The chemistry and mineralogy of some South Australian calcretes and associated soft carbonates and their dolomitisation. Journal of the Geological Society of Australia 28(1-2): 71-79.

Jacobson, G, Arakel, A, Yijian, C. 1988. The central Australian groundwater discharge zone: evolution of associated calcrete and gypcrete deposits. Australian Journal of Earth Sciences 35(4): 549-565.

Jin, L, Siegel, DI, Lautz, LK, Mitchell, MJ, Dahms, DE, Mayer, B. 2010. Calcite precipitation driven by the common ion effect during groundwater–surface-water mixing: A potentially common process in streams with geologic settings containing gypsum. Geological Society of America Bulletin 122(7-8):1027-1038.

Kadir, S, Eren, M, Atabey, E. 2010. Dolocretes and associated palygorskite occurrences in siliciclastic red mudstones of the Sariyer formation (Middle Miocene), southeastern side of the Çanakkale strait, Turkey. Clays and Clay Minerals 58(2): 205-219.

Khalaf, FI. 1990. Occurrence of phreatic dolocrete within Tertiary clastic deposits of Kuwait, Arabian Gulf. Sedimentary Geology 68(3): 223-239.

Khalaf, FI, Abdal, MS. 1993. Dedolomitization of dolocrete deposits in Kuwait, Arabian Gulf. Geologische Rundschau 82(4): 741-749.

Khalaf, FI, Abdullah, FA, Gharib, IM. 2017. Petrography, diagenesis and isotope geochemistry of dolostones and dolocretes in the Eocene Dammam Formation, Kuwait, Arabian Gulf. Carbonates and Evaporites. DOI 10.1007/s13146-016-0330-5.

Killick, M, Churchward, H, Anand, R. 2008. Regolith terrain analysis for iron ore exploration in the Hamersley Province, Western Australia. CRC-LEME open file report 214, CSIRO Exploration and Mining, Perth, Australia.

Kneeshaw, M, Morris, RC. 2014. The Cenozoic detrital iron deposits of the Hamersley Province, Western Australia. Australian Journal of Earth Sciences 61(4): 513-586.

Land, LS. 1998. Failure to Precipitate Dolomite at 25° C from Dilute Solution Despite 1000-Fold Oversaturation after 32 Years. Aquatic Geochemistry 4(3): 361-368.

Last, WM. 1990. Lacustrine dolomite—an overview of modern, Holocene, and Pleistocene occurrences. Earth-Science Reviews 27(3): 221-263.

Lippmann, F., 1973. Sedimentary Carbonate Minerals, Rocks, and Inorganic Materials. Monograph Series of Theoretical and Experimental Studies Vol. 4 Springer-Verlag, Berlin (228 p).

Macphail, M, Stone, M. 2004. Age and palaeoenvironmental constraints on the genesis of the Yandi channel iron deposits, Marillana Formation, Pilbara, northwestern Australia. Australian Journal of Earth Sciences 51(4): 497-520.

Mann, AW, Deutscher, RL. 1978. Hydrochemistry of a calcrete-containing aquifer near Lake Way, Western Australia. Journal of Hydrology 38: 357-377.

Mann, A, Horwitz, R. 1979. Groundwater calcrete deposits in Australia some observations from Western Australia. Journal of the Geological Society of Australia 26(5-6): 293-303.

Mather, CC, Skrzypek, G, Dogramaci, S, Grierson, PF. 2018. Paleoenvironmental and paleohydrochemical conditions of dolomite formation within a saline wetland in arid northwest Australia. Quaternary Science Reviews 185: 172-188.

McCallum, JL, Dogramaci, S, Cook, PG, Banks, E, Purtschert, R, Irvine, M, Simmons, C, Burk, L. 2018. Stochastic correction of carbon-14 activities: A Bayesian approach with argon-39 validation. Journal of Hydrology 566: 396-405.

Mook, WG, Bommerson, JC, Staverman, WH. 1974. Carbon isotope fractionation between dissolved bicarbonate and gaseous carbon dioxide. Earth and Planetary Science Letters 22(2): 169-176.

Morris, RC. 1993. Genetic modelling for banded iron-formation of the Hamersley Group, Pilbara Craton, Western Australia: Precambrian Research 60(1): 243-286.

Morris, RC, Ramanaidou, ER. 2007. Genesis of the channel iron deposits (CID) of the Pilbara region, Western Australia. Australian Journal of Earth Sciences 54: 733-765.

Morrow, DW. 1982. Diagenesis 1. Dolomite-Part 1: the chemistry of dolomitization and dolomite precipitation. Geoscience Canada 9 (1): 5-13.

Nash, DJ, McLaren, SJ. 2003. Kalahari valley calcretes: their nature, origins, and environmental significance: Quaternary International 111(1): 3-22.

Pain, CF, Ollier, CD. 1995. Inversion of relief – a component of drainage evolution. Geomorphology 12: 151-165.

Parkhurst, DL, Appelo, C, 1999. User's guide to PHREEQC (Version 2): A computer program for speciation, batch-reaction, one-dimensional transport, and inverse geochemical calculations. Water Resources Investigations Report 99-4259, U.S. Department of the Interior and U.S. Geological Survey, Denver, Colorado.

Paul, D, Skrzypek, G. 2007. Assessment of carbonate-phosphoric acid analytical technique performed using GasBench II in continous flow isotope mass spectrometry. International Journal of Mass Spectrometry 262(3): 180-186.

Petrash, DA, Bialik, OM, Bontognali, TRR, Vasconcelos, C, Roberts, JA, McKenzie, JA, Konhauser, KO. 2017. Microbially catalyzed dolomite formation: From near-surface to burial. Earth-Science Reviews 171: 558-582.

Petersen, MNA, Bien, GS, Berner, RA. 1963. Radiocarbon Studies of Recent Dolomite from Deep Spring Lake, California. Journal of Geophysical Research 68(24) 6493-6506.

Reeder, RJ, Sheppard, CE. 1984. Variation of lattice parameters in some sedimentary dolomites. American Mineralogist 69(5-6): 520-527.

Roberts, JA, Kenward, PA, Fowle, DA, Goldstein, RH, González, LA, Moore, DS. 2013. Surface chemistry allows for abiotic precipitation of dolomite at low temperature. Proceedings of the National Academy of Sciences 110(36): 14540-14545.

Rouillard, A, Skrzypek, G, Dogramaci, S, Turney, C, Grierson, PF. 2015. Impacts of high inter-annual variability of rainfall on a century of extreme hydrologic

regime of northwest Australia. Hydrology and Earth System Sciences 19(4): 2057-2078.

Sanz-Rubio, E, Sánchez-Moral, S, Cañaveras, JC, Calvo, JP, Rouchy, JM. 2001. Calcitization of Mg–Ca carbonate and Ca sulphate deposits in a continental Tertiary basin (Calatayud Basin, NE Spain). Sedimentary Geology 140(1): 123-142.

Schmidt, PW, Williams, GE. 2017. Paleomagnetic age of ferruginous weathering beneath the Hamersley Surface, Pilbara, Western Australia, and the Cenozoic apparent polar wander path. Australian Journal of Earth Science 64(2): 239-249.

Sibley, DF, Gregg, JM. 1987. Classification of dolomite rock textures. Journal of Sedimentary Petrology 57(6): 967-975.

Simonson, BM, Schubel, KA, Hassler, SW. 1993. Carbonate sedimentology of the early Precambrian Hamersley Group of Western Australia. Precambrian Research (60): 287-335.

Skrzypek, G. 2013. Normalization procedures and reference material selection in stable HCNOS isotope analyses: an overview. Analytical and bioanalytical chemistry 405(9): 2815-2823.

Skrzypek, G, Dogramaci, S, Grierson, PF. 2013. Geochemical and hydrological processes controlling groundwater salinity of a large inland wetland of northwest Australia. Chemical Geology 357: 164-177.

Spadafora, A, Perri, E, McKenzie, JA, Vasconcelos, C. 2010. Microbial biomineralization processes forming modern Ca: Mg carbonate stromatolites: Sedimentology 57(1): 27-40.

Spötl, C, Wright, VP. 1992. Groundwater dolocretes from the Upper Triassic of the Paris Basin, France: a case study of an arid, continental diagenetic facies: Sedimentology 39(6): 1119-1136.

Talbot, M. 1990. A review of the palaeohydrological interpretation of carbon and oxygen isotopic ratios in primary lacustrine carbonates. Chemical Geology: Isotope Geoscience Section 80(4): 261-279.

Thomas, MF. 1994. Geomorphology in the Tropics: Study of Weathering and Denudation in Low Latitudes. Wiley, Chichester.

Trendall, AF. 1968. Three great basins of Precambrian banded iron formation deposition: a systematic comparison: Geological Society of America Bulletin 79(11): 1527-1544.

Trendall, AF, Blockey, J. 1970. The iron formations of the Precambrian Hamersley Group, Western Australia with special reference to the associated crocidolite, Geological Survey of Western Australia Bulletin 119.

Trendall, AF, Compston, W, Nelson, DR, De Laeter, JR, Bennett, VC. 2004. SHRIMP zircon ages constraining the depositional chronology of the Hamersley Group, Western Australia. Australian Journal of Earth Sciences 51(5): 621-644.

Tucker, ME. 1991. Sedimentary Petrology: an Introduction to the Origin of Sedimentary Rocks. (2nd edition). Blackwell-Scientific, Oxford.

Twidale, CR, Horwitz, RC, Campbell, EM. 1985. Hamersley landscapes of the northwest of Australia. Revue de Geologie Dynamique et de Geographie Physique 26: 173-186.

Van Lith, Y, Vasconcelos, C, Warthmann, R, Martins, JCF, McKenzie, JA. 2002. Bacterial sulphate reduction and salinity: two controls on dolomite precipitation

in Lagoa Vermelha and Brejo do Espinho (Brazil). Hydrobiologia 485 (1): 35-49.

Vasconcelos, C, McKenzie, JA, Bernasconi, S, Grujic, D, Tien, AJ. 1995. Microbial mediation as a possible mechanism for natural dolomite formation at low temperatures. Nature 377: 220-222.

Vasconcelos, C, McKenzie, JA. 1997. Microbial mediation of modern dolomite precipitation and diagenesis under anoxic conditions (Lagoa Vermelha, Rio de Janeiro, Brazil). Journal of Sedimentary Research 67(3): 378-390.

Vasconcelos, C, McKenzie, JA, Warthmann, R, Bernasconi, SM. 2005. Calibration of the $\delta^{18}O$ paleothermometer for dolomite precipitated in microbial cultures and natural environments. Geology 33(4): 317-320.

Von der Borch, C. C., 1976, Stratigraphy and formation of Holocene dolomitic carbonate deposits of the Coorong area, South Australia. Journal of Sedimentary Petrology 46(4) 952-966.

Wacey, D., Wright, DT, Boyce, AJ. 2007. A stable isotope study of microbial dolomite formation in the Coorong Region, South Australia. Chemical Geology 244(1): 155-174.

Wanas, HA, Sallam, E. 2016. Abiotically-formed, primary dolomite in the mid-Eocene lacustrine succession at Gebel El-Goza El-Hamra, NE Egypt: An approach to the role of smectitic clays. Sedimentary Geology 343:132-140.

Wright, VP. 2007. Calcrete. In: Nash, DJ, McLaren, SJ (Eds). Geochemical Sediments and Landscapes. Wiley-Blackwell, Oxford: 10-45.

Wright, VP, Tucker, ME. 1991. Calcretes, Blackwell Scientific Publications.

Zhang, F, Xu, H, Konishi, H, Shelobolina, ES, Roden, EE. 2012. Polysaccharide-catalyzed nucleation and growth of disordered dolomite: A potential precursor of sedimentary dolomite. American Mineralogist 97(4): 556-567.

Zhang, F, Xu, H, Shelobolina, ES, Konishi, H, Converse, B, Shen, Z, Roden, EE. 2015. The catalytic effect of bound extracellular polymeric substances excreted by anaerobic microorganisms on Ca-Mg carbonate precipitation: Implications for the “dolomite problem”. American Mineralogist 100(2-3): 483-494.

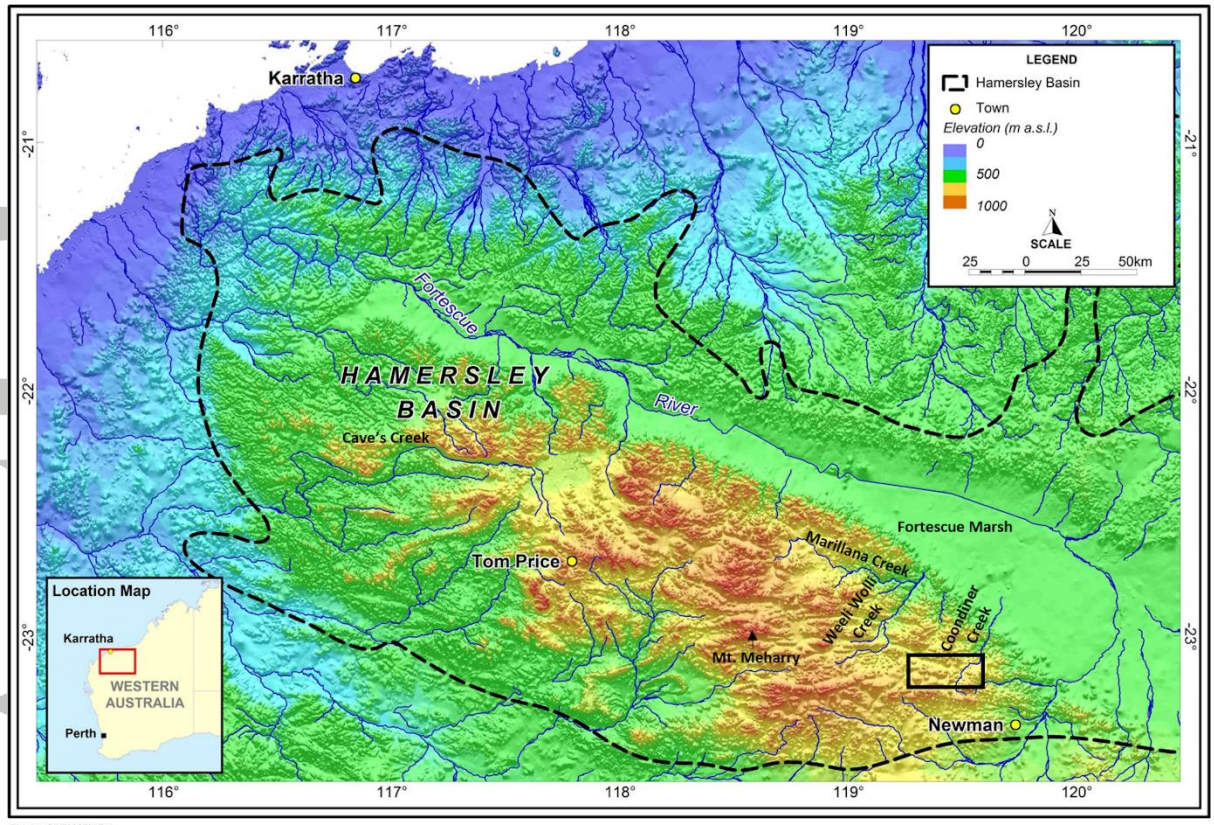

Figure 1: Digital elevation map of the Hamersley Basin with major drainage overlaid. The inset shows the Hamersley Basin location within Western Australia. Black rectangle shows study area presented in Figure 3.

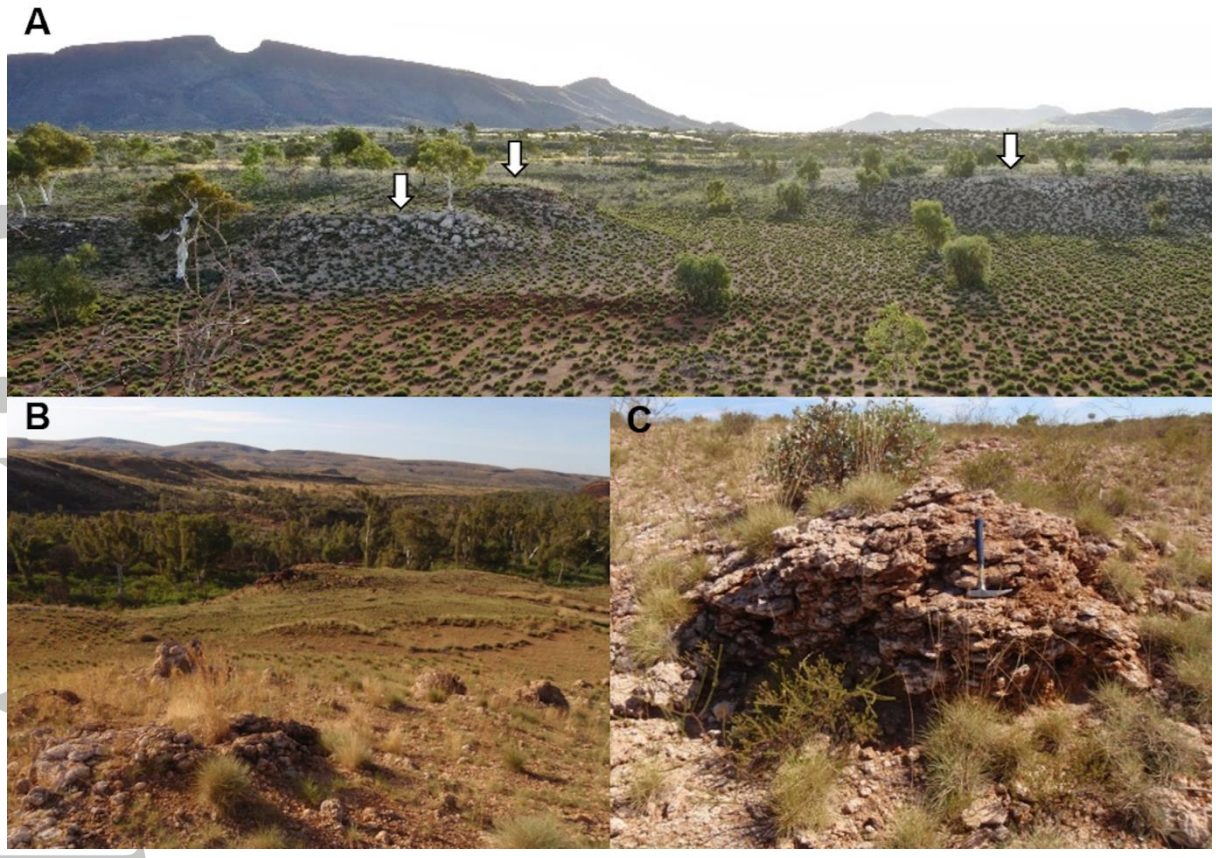

Figure 2: View of dolocrete within the Hamersley Basin landscape. A) Dolocrete mounds (indicated by arrows) extruding several metres above the valley floor close to Cave's Creek. B) Eroding dolocrete mound in relative upland position, looking northwest towards Coondiner Creek. C) Eroding dolocrete outcrop, proximal to Coondiner Creek within the study area.

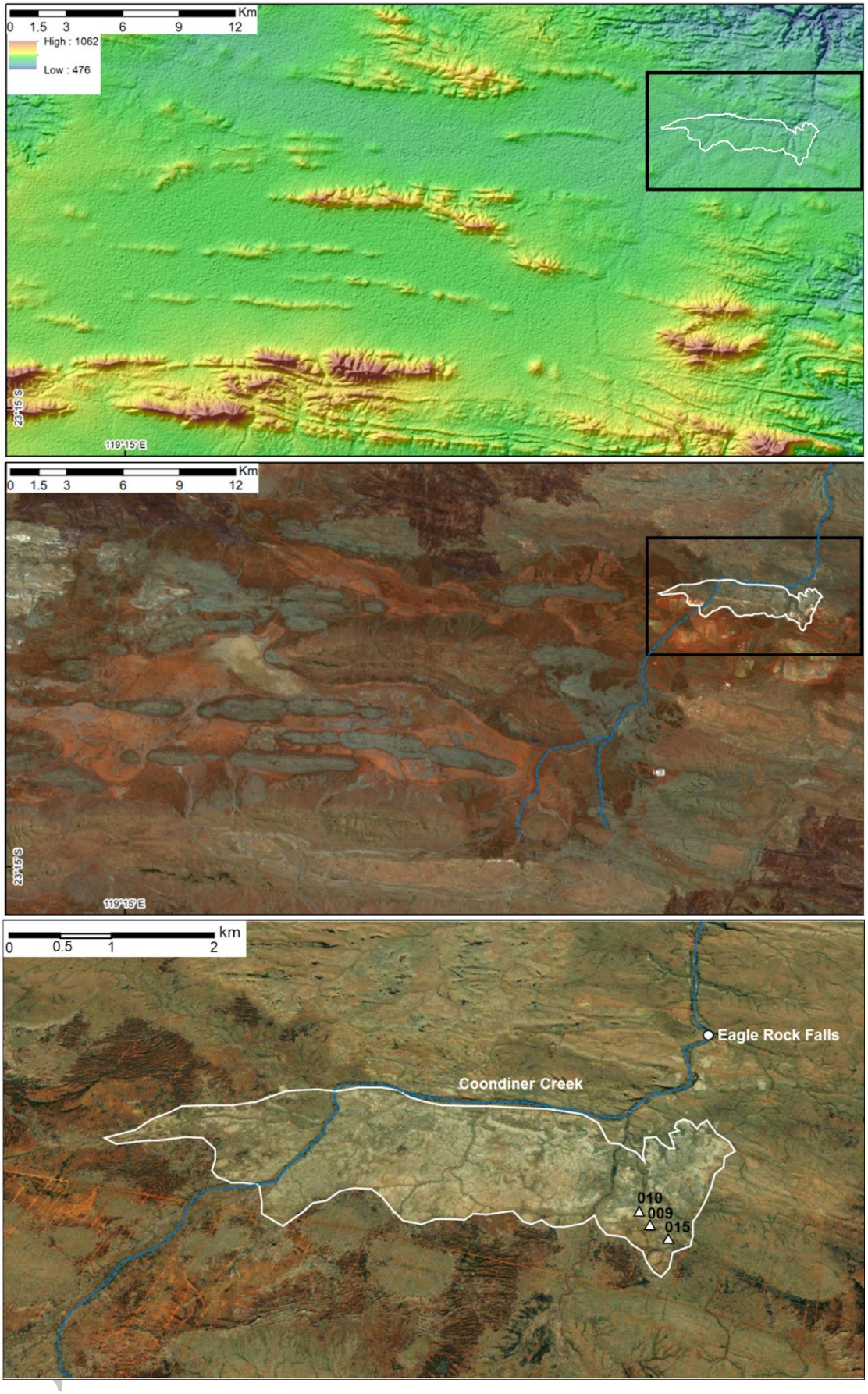

Figure 3: A) Digital elevation map (exaggeration *2.5) and B) true colour aerial photography showing the study area within Coondiner Creek sub-catchment. Coondiner creek is indicated by the dotted line. The dolocrete outcrop is outlined in white and the black rectangle indicates the area shown in; C) A higher magnification aerial view of the dolocrete outcrop (outlined in white) within the study area and location of drill cores used for this study (Google Earth, 2007 – pre-mining).

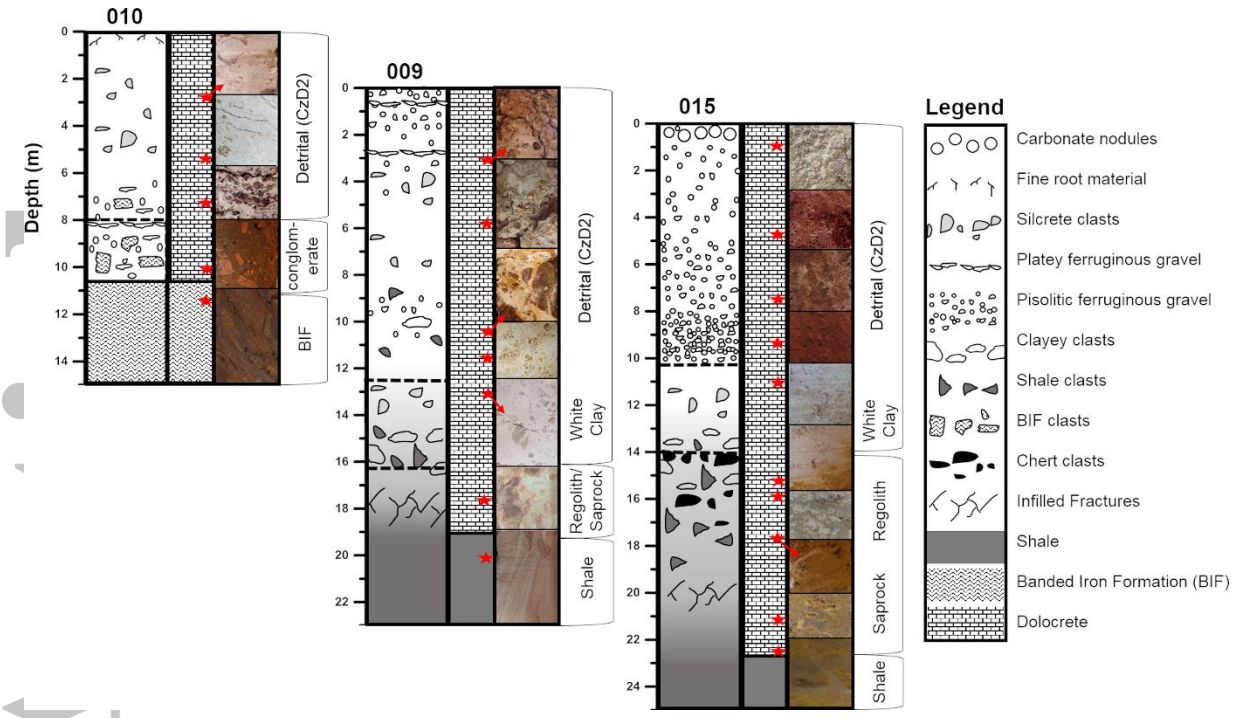

Figure 4: The host sediment profiles and extent of dolocrete within cores 009 and 015 overlying McRae Shale and core 010 upon Joffre member banded iron formation (BIF) of the Brockman Iron Formation. Detrital sediments are classified as CzD2 after Kneeshaw and Morris (2014) and comprise lacustrine and alluvial sediments. The right hand side of each log shows the subdivision between dolocrete and bedrock. Regolith includes all in-situ developed regolith and saprolite. Saprock refers to in-situ weathered bedrock, with abundant primary textures but mineralogy that is distinct from fresh bedrock. Grey shading indicates the transition from dolocrete to primary shale minerals and texture. Photographs of core sections (all 6 cm diameter) representing different sediment characteristics are displayed alongside, with the depth indicated by red stars.

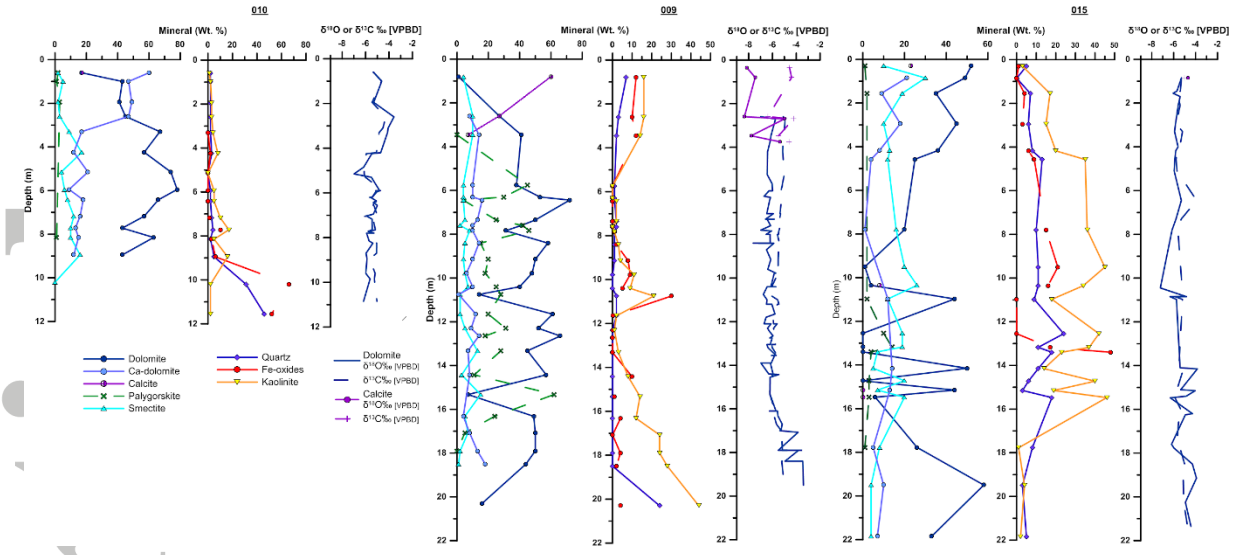

Figure 5: Mineralogy and stable C and O isotope compositions of core profiles. Mineralogy was determined from bulk samples by XRD, and only the major mineral assemblage is shown. Fe-oxides are the sum of hematite and goethite. Carbonate $\delta^{18}O$ and $\delta^{13}C$ values did not vary notably for different sub-sample groups and are included along with bulk isotope data.

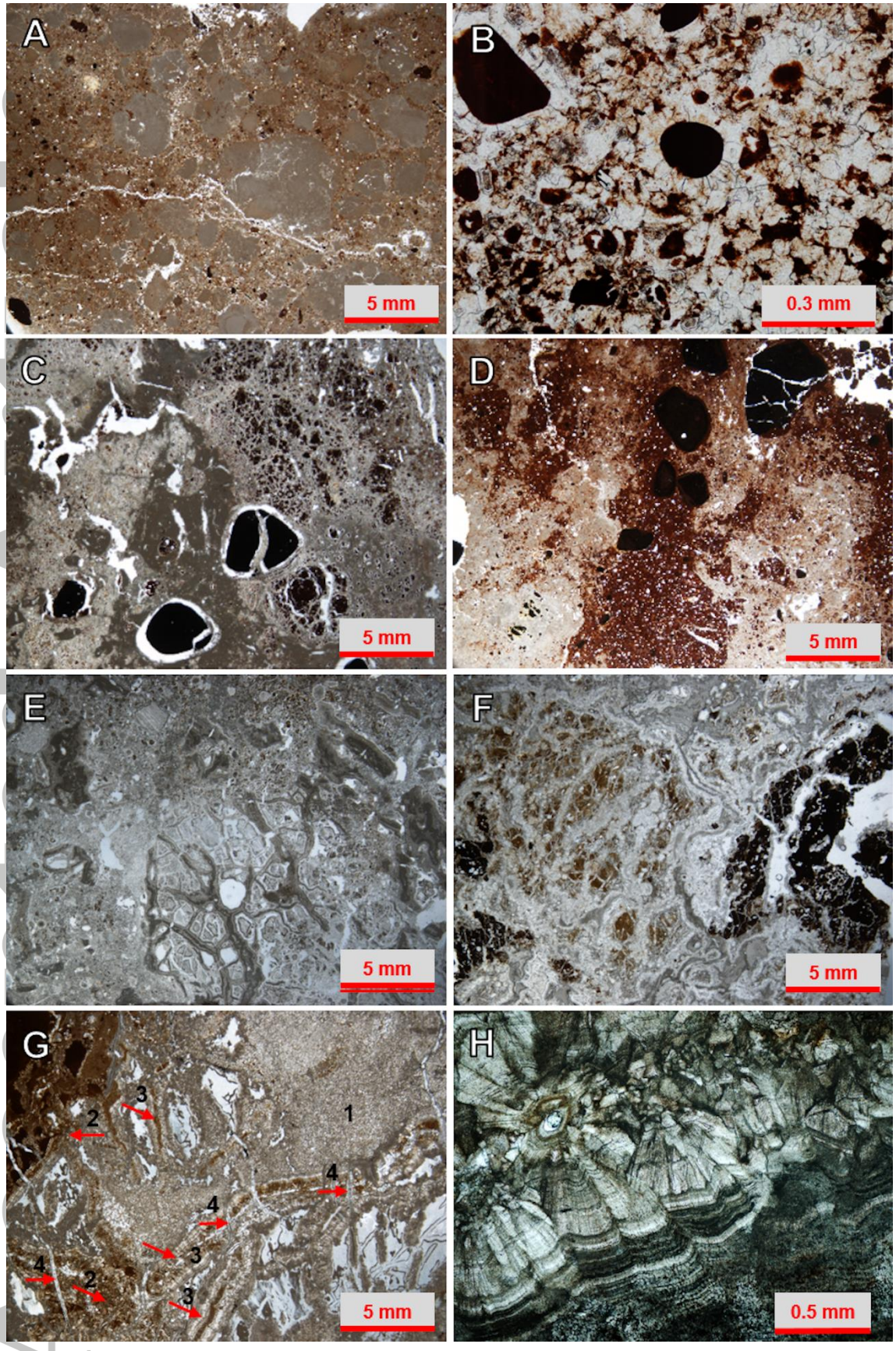

Figure 6: Optical photomicrographs of dolocrete thin sections showing variation in textures within profiles. Micrographs were imaged using a binocular microscope unless otherwise indicated. A: Core 015 (0.3m depth) Pedogenic nodules of dense dolomicrite developed within carbonate and clay matrix. B: Core 009 (2.6 m depth) Plane-polarised micrograph of blocky phreatic dolomite cement surrounding pisolitic gravel and fragments within cemented matrix of similar size dolomite (~50 µm) of planar-s fabric. Fe-staining of dolomite and some relict detrital sediment occurs within the matrix. C: Core 010 (7.2m depth) Pisolitic gravel and fine Fe-rich sediments within dolomicrite matrix, finely mingled with smectite and kaolinite. Coarse voids, up to ~1 mm wide, surround pisoliths and occur within the matrix, appear to be from desiccation. Voids are lined with dolomite cement. D: Core 015 (7.8m depth) Dolomite cement and replacement within hematite- and kaolin-rich sediment. The red-brown matrix is largely kaolinite with Fe-staining where Fe has dissolved, whereas pisolitic gravel remains intact. Dolomite has preferentially infilled zones and is heterogeneous, shown by cream coloured matrix. E: Core 015 (11 m depth) Brecciated and cemented dolocrete. Dolocrete fabrics have been fragmented and occur within dolomite and clay (kaolinite and smectite) matrix. F: Core 015 (14.2 m depth) Multiple generations of dolomite cement within saprolite of shale, showing laminar dolomite cement within fissures and solution pipes cross-cutting some weathered shale fragments and earlier dolomite. G: Core 009 (17.1 m depth) Shale saprolite to saprock, showing a highly altered zone with multiple generations of dolomite including greyish-brown planar-s matrix (1), Fe-stained spheroidal dolomite (2) and curvilinear laminar Fe-stained cements (3), which have been cross-cut by later fissures (4). The laminar cements and infilled fissures appear to be features of bioturbation from roots or burrowing. Deci-micron-scale veinlets connect through pore spaces. The saprock dolomite textures are

distinct from overlying dolocrete textures and could reflect primary marine textures. H: Core 009 (18 m depth) Plane-polarised micrograph of spheroidal dolomite and fan-like radial morphologies with concentric zoning within saprock. These textures occur in the curvilinear structures shown in G – 4.

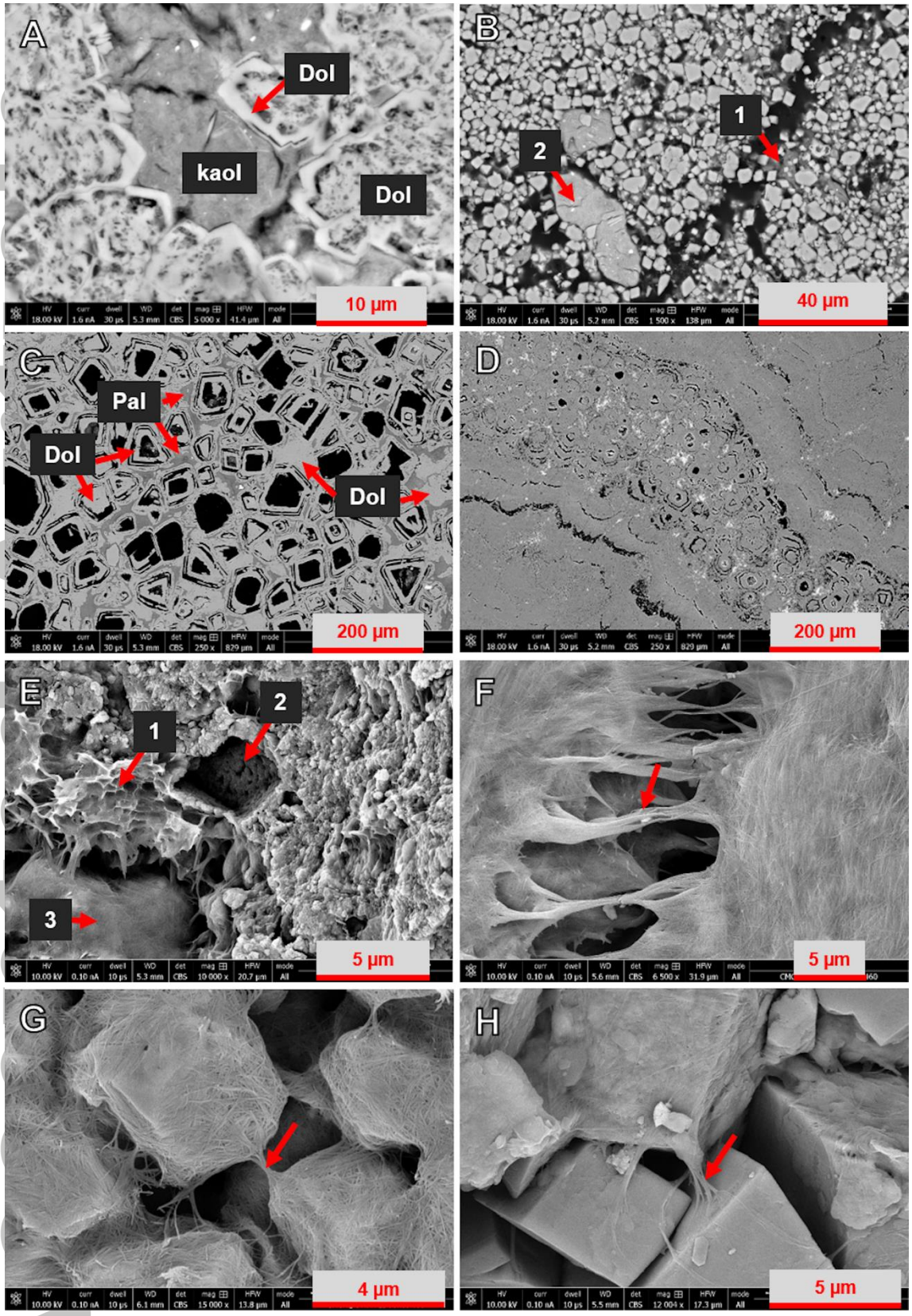

Figure 7: Scanning electron backscatter micrographs showing examples of dolomite morphologies and associated textures. Dol=dolomite, Kaol=kaolinite,

Pal=palygorskite. A: Core 010 (3.3 m depth) Partly dissolved dolomite showing what appear to be smaller dolomite crystals forming a larger rhomb, where further dolomite has precipitated around the edges forming rhombic overgrowth. Dolomite surrounds detrital kaolinite. B: Core 010 (4.2 m depth) Subhedral to euhedral dolomite mingled with smectite (1) and some detrital kaolinite-dominated clasts (2). C: Core 009 (12.7 m depth) Advanced dissolution of dolomite cores and zones. This image shows microporosity developed as dissolved dolomite zones remain open. Palygorskite occurs between dolomite rhombs. D: Core 009 (17.1 m depth) Fe-stained zoned dolomite cement forming curvilinear structures through a dolomite matrix within saprock. Fe-oxides (white precipitate) occur within some voids and account for some of the brown colouring of the cement. E: Core 015 (0.9 m depth) Micritic dolomite mingled with clays, showing; (1) fossilised honeycomb texture of microbial EPS; (2) void remaining from dissolution of dolomite rhomb and; (3) fibrous clay coating over crystals. F: Core 009 (6 m depth) Fossil organic filaments connecting across pore space between interwoven fibrous clay. G: Core 010 (9 m depth) Dolomite rhombs coated by fibrous clays, connected by fossilised organic filaments. Arrow indicates organic filament after EPS. H: Core 015 (11.1 m depth) Dolomite rhombs with some coating by fibrous clay. Arrow indicates organic filament after EPS.

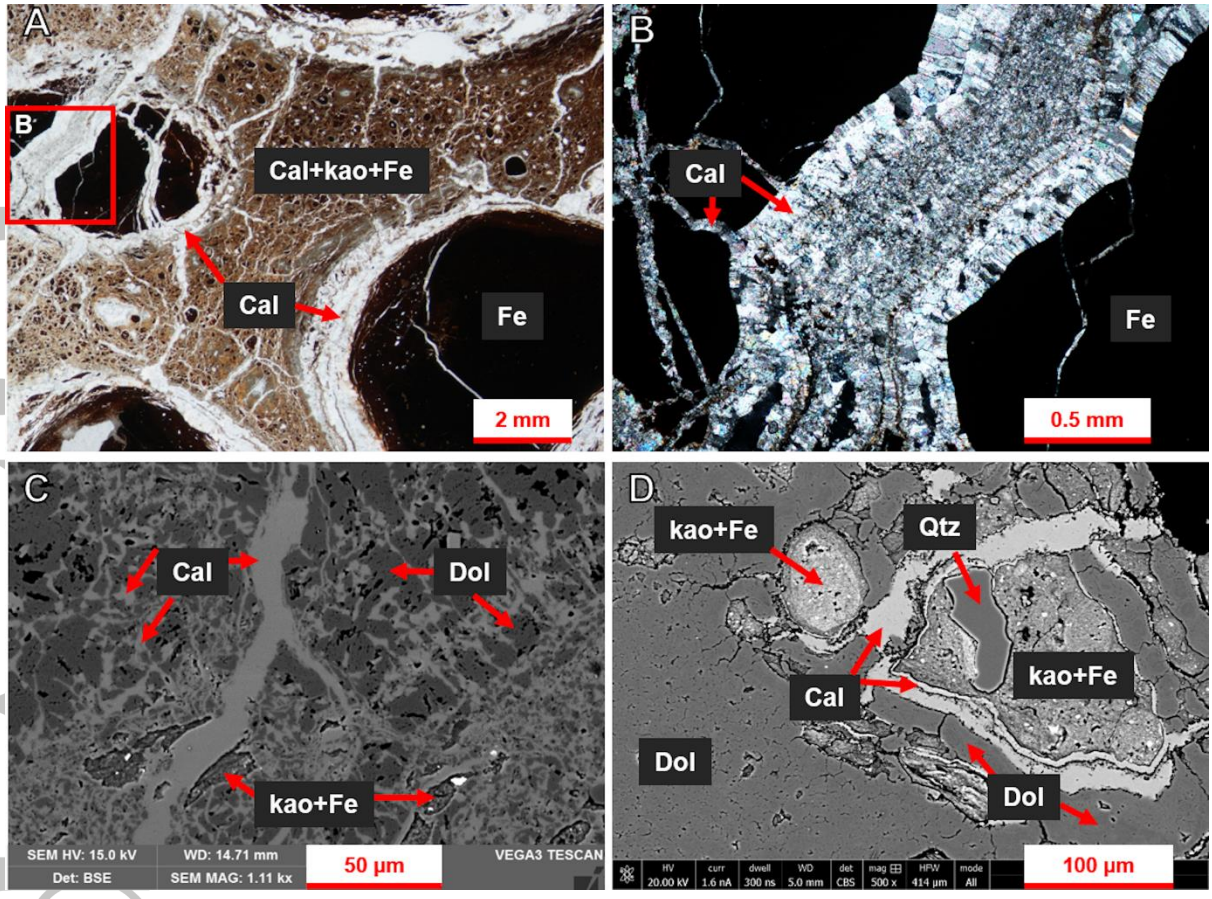

Figure 8: Calcite cement and replacement of dolomite within top 3 m of Core 009. Cal=calcite, Dol=dolomite, Cla=clay, Fe=Fe-oxides, Qtz=quartz. A: Core 009 (0.8 m depth) Binocular micrograph of calcite cement within voids surrounding pisolitic gravel and infilling fractures through pisoliths and matrix. Dolomite within the matrix has been largely replaced by calcite. Red box shows location of image B. B: Core 009 (0.8 m depth) Optical micrograph with cross-polarised light showing calcite infill of fractures through a pisolith. Coarser cements line the fracture walls and become finer and micritic towards the centre of the fracture. C: Core 009 (0.8 m depth) SEM micrograph showing calcite infill of finer fractures within dolomite matrix. Dolomite has microporosity and it appears there may be some dissolution and replacement by calcite within the finer pores. D: Core 009 (2.6 m depth) SEM micrograph showing calcite infill of void surrounding detrital material within larger dolomite matrix.

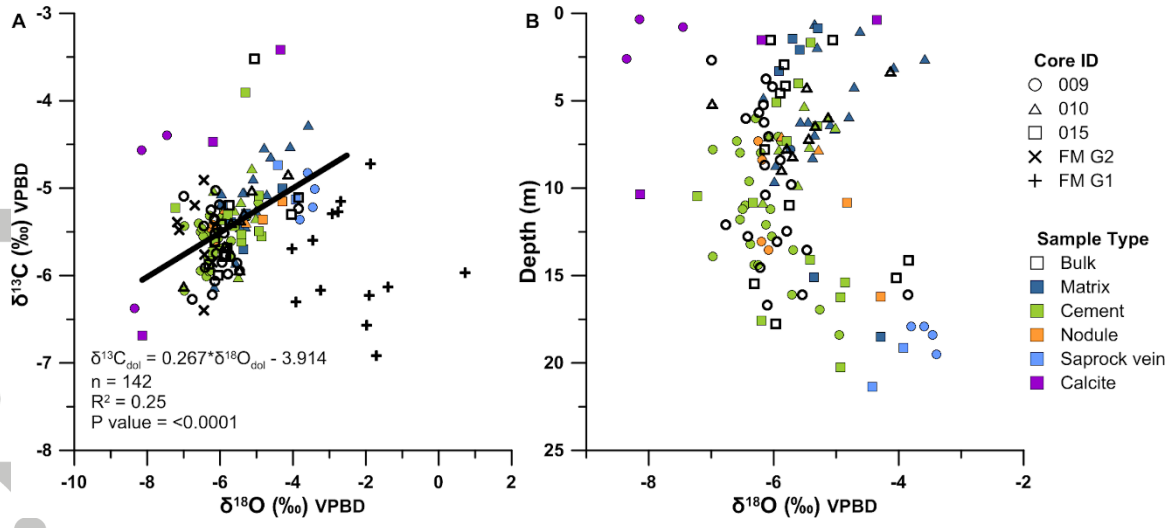

Figure 9: A: Stable carbon and oxygen isotope values for Coondiner dolocrete samples, with linear regression statistics shown for the relationship between dolomite $\delta^{13}C$ and $\delta^{18}O$. Results for the nearby Fortescue Marsh (FM) dolomite (data from Mather et al., 2018) are shown for comparison. B: Stable oxygen isotope values for Coondiner dolocrete samples shown with depth.

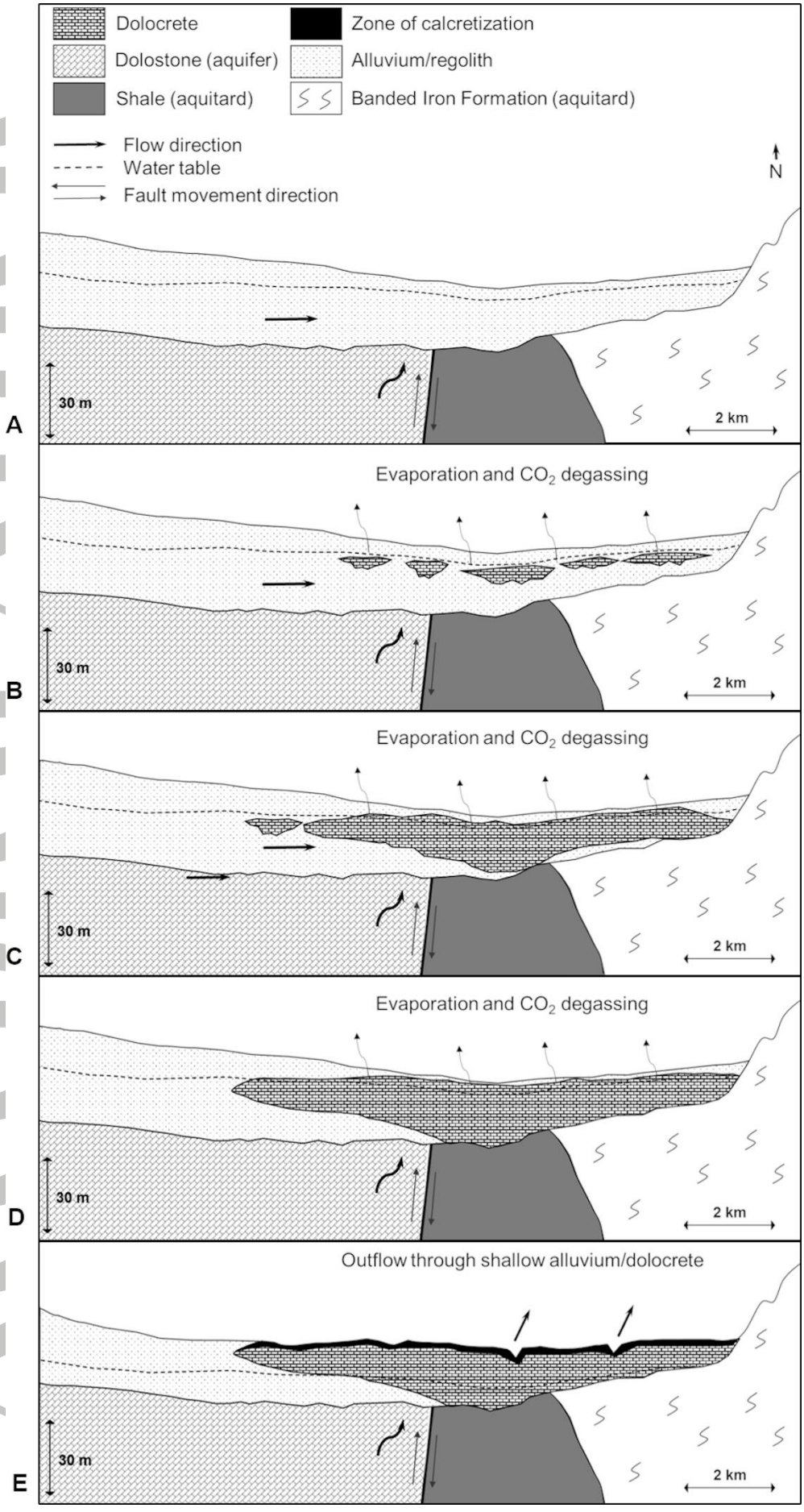

Figure 10: Schematic cross-section of study area showing the stages of dolocrete formation and landform evolution in an upland area of the Hamersley Basin. A: Broad shallow groundwater system in internally draining sub-basin. B: Initial dolomite precipitation, promoted by evaporation and CO_2 degassing from shallow Mg-rich groundwater. C: Displacive growth of dolocrete, building up and outward. D: Continued growth of dolocrete to form larger body, extending throughout sediment profile and towards the surface. E: The modern setting; a relatively lower water table and erosion and incision of dolocrete by modern drainage. Groundwater outflow to Coondiner Creek. Calcretization and dissolution of dolomite occurring close to the surface.